Article

Cell Stem Cell

Epigenetic Restoration of Fetal-like IGF1 Signaling Inhibits Leukemia Stem Cell Activity

Graphical Abstract

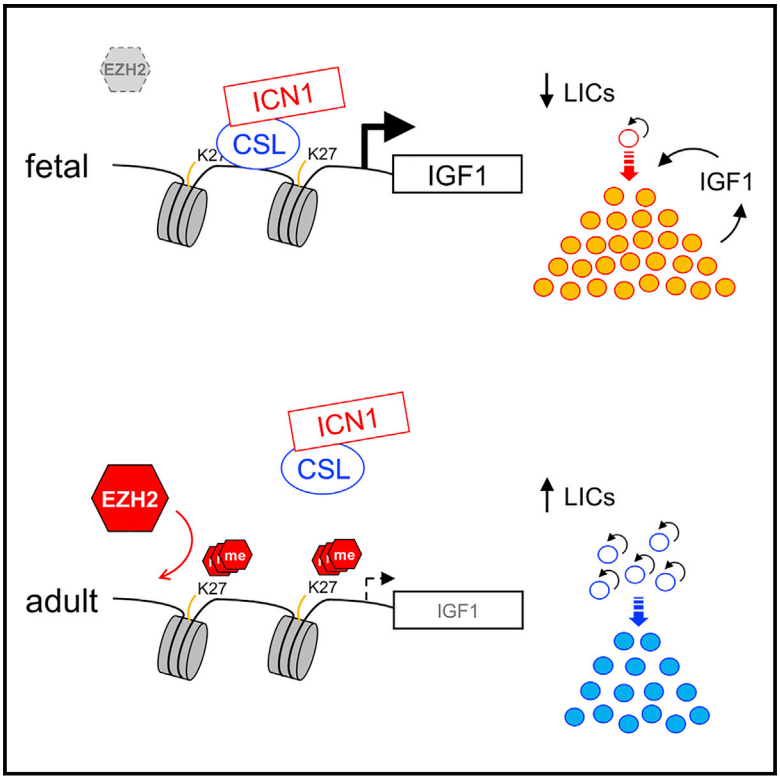

Highlights

- NOTCH1 leukemias derived from fetal liver are less transplantable than those from BM
- NOTCH1 promotes auto/paracrine IGF1 signaling in fetal liver, but not BM progenitors
- H3K27 methylation by EZH2 blocks NOTCH1 from accessing the *IGF1* promoter in BM cells
- Enforced IGF1 signaling depletes leukemia stem cells in both mouse and human T-ALL

Authors

Vincenzo Giambra, Samuel Gusscott, Deanne Gracias, ..., Martin Hirst, Connie J. Eaves, Andrew P. Weng

Correspondence

vgiambra@bccrc.ca (V.G.), aweng@bccrc.ca (A.P.W.)

In Brief

Giambra et al. show that NOTCH1 leukemias generated from fetal liver are less transplantable than those from adult bone marrow. NOTCH1 activates auto/paracrine IGF1 signaling in FL, but not BM cells, due to EZH2-dependent H3K27 trimethylation at the *IGF1* promoter. This mechanism can be exploited to exhaust/deplete leukemia stem cells.

Giambra et al., 2018, Cell Stem Cell *23*, 714–726
November 1, 2018
https://doi.org/10.1016/j.stem.2018.08.018

CellPress

CellPress

Cell Stem Cell
Article

Epigenetic Restoration of Fetal-like IGF1 Signaling Inhibits Leukemia Stem Cell Activity

Vincenzo Giambra,[1,2,*] Samuel Gusscott,[1] Deanne Gracias,[1] Raymond Song,[1] Sonya H. Lam,[1] Patrizio Panelli,[2] Kateryna Tyshchenko,[1] Catherine E. Jenkins,[1] Catherine Hoofd,[1] Alireza Lorzadeh,[3] Annaick Carles,[3] Martin Hirst,[3] Connie J. Eaves,[1] and Andrew P. Weng[1,4,*]

[1]Terry Fox Laboratory, BC Cancer Agency, Vancouver, BC V5Z 1L3, Canada

[2]Institute for Stem Cell Biology, Regenerative Medicine and Innovative Therapies (ISBReMIT), Fondazione IRCCS Casa Sollievo della Sofferenza, 71013 San Giovanni Rotondo (FG), Italy

[3]Michael Smith Laboratories and Department of Microbiology and Immunology, University of British Columbia, Vancouver, BC V6T 1Z4, Canada

[4]Lead Contact

*Correspondence: vgiambra@bccrc.ca (V.G.), aweng@bccrc.ca (A.P.W.)

https://doi.org/10.1016/j.stem.2018.08.018

SUMMARY

Acute leukemias are aggressive malignancies of developmentally arrested hematopoietic progenitors. We sought here to explore the possibility that changes in hematopoietic stem/progenitor cells during development might alter the biology of leukemias arising from this tissue compartment. Using a mouse model of acute T cell leukemia, we found that leukemias generated from fetal liver (FL) and adult bone marrow (BM) differed dramatically in their leukemia stem cell activity with FL leukemias showing markedly reduced serial transplantability as compared to BM leukemias. We present evidence that this difference is due to NOTCH1-driven autocrine IGF1 signaling, which is active in FL cells but restrained in BM cells by EZH2-dependent H3K27 trimethylation. Further, we confirmed this mechanism is operative in human disease and show that enforced IGF1 signaling effectively limits leukemia stem cell activity. These findings demonstrate that resurrecting dormant fetal programs in adult cells may represent an alternate therapeutic approach in human cancer.

INTRODUCTION

Acute leukemias are aggressive malignancies of developmentally arrested hematopoietic progenitors that require immediate treatment, usually consisting of multi-agent chemotherapy (De Kouchkovsky and Abdul-Hay, 2016; Terwilliger and Abdul-Hay, 2017). Large-scale sequencing studies have identified a host of genetic alterations as candidate therapeutic targets that are currently making their way into clinical trials design. Parallel efforts have emphasized the effect of cell of origin on tumor biology (Visvader, 2011), mostly notably germinal center versus activated B cell types of diffuse large B cell lymphoma (Alizadeh et al., 2000) and basal versus luminal types of breast cancer (Perou et al., 2000). Cell-of-origin studies in acute myeloid leukemia have yielded insights into hematopoietic stem versus progenitor-derived tumors, which have distinct chromatin landscapes and clinical outcomes (George et al., 2016; Krivtsov et al., 2013). In T cell acute lymphoblastic leukemia (T-ALL), tumors with gene expression profiles similar to normal early T cell precursors (ETPs) were shown to have a high risk of remission failure compared to typical T-ALL (Coustan-Smith et al., 2009). While the concept of cell of origin in cancer has most often been invoked with respect to cell lineage, histologic type, or stage of differentiation, it remains unclear to what extent differences in age-related gene expression/functional programs may contribute to diversity in biological behavior and ultimately in clinical responses to therapy.

During hematopoietic ontogeny, there are well-documented shifts in the properties of hematopoietic stem cells (HSCs) as the organism transitions from fetal to post-natal life and beyond. Aging-associated changes include features such as diminished adaptive immunity, increased HSC numbers yet with reduced regenerative potential, and progressive myeloid bias (Snoeck, 2013). Multiple groups have characterized that functional properties of HSC switch abruptly from fetal to adult patterns early in life (between 2 and 4 weeks of age in mice) and overall reinforce the notion that HSC transition from actively proliferating to quiescent states around the time of birth (Babovic and Eaves, 2014). The majority of mechanisms underlying HSC aging are thought to be primarily cell intrinsic, although a limited number of studies have begun to characterize cell-extrinsic mechanisms as well (Geiger et al., 2013; Kanzler et al., 1996). Fetal and adult HSCs exhibit distinct transcriptional programs (Copley et al., 2013; Kim et al., 2007; Oshima et al., 2016; Yuan et al., 2012) with genes including *Sox17*, *Lin28b/let-7*, *Hmga2*, *Ezh2*, *Pten*, *Bmi1*, and *Cebpa* having been identified to play dominant roles in mediating fetal/adult-specific phenotypes (Babovic and Eaves, 2014). These age-related gene programs yield not only quantitative differences in output lineages, but also qualitative differences in the functional properties of mature subsets. For instance, fetal $CD4^+$ T cells are more tolerogenic than adult $CD4^+$ T cells (Mold et al., 2010), and fetal $CD8^+$ T cells are more likely to become effector over memory cells while adult $CD8^+$ T cells exhibit the opposite tendency (Wang et al., 2016). With these age-related differences among normal HSCs and

their differentiated progeny in mind, we sought to explore whether hematopoietic stem/progenitor cells (HSPCs) from different stages of life might yield leukemias with distinct biological properties.

NOTCH1 is a prominent oncogene in T-ALL and is activated by mutation in over 50% of cases (Weng et al., 2004). One of the most widely utilized mouse models of T-ALL involves viral transduction/transplantation of bone-marrow-derived HSPC with activated NOTCH1 (Giambra et al., 2012, 2015; Medyouf et al., 2010, 2011; Pear et al., 1996). Bone marrow donors for these experiments are typically adult mice ranging from 8 to 12 weeks of age, and thus these studies could be interpreted as having modeled disease emanating from adult-program cells. We sought therefore to determine what, if any, differences would arise if we were to use fetal-program cells as the donor source material instead. We report here striking phenotypic differences between NOTCH1-transduced FL and bone marrow (BM) HSPCs, which are perpetuated through to their respective derived leukemias. Additionally, we identified the underlying mechanism to include epigenetic regulation of insulin growth factor (IGF) signaling, which we were able to reverse and thus enforce fetal-like phenotypes in adult cells. Finally, we provide proof of concept that invoking otherwise extinct fetal-like programs in human T-ALL cells can dramatically alter their biological behavior in a manner that recapitulates features of the mouse FL/BM dichotomy.

RESULTS

Leukemias Derived from Fetal Liver Are Characterized by Poor Transplantability and Rapid Cycling

It is well established that normal fetal hematopoiesis differs qualitatively from that which occurs in adulthood, and that many of these features are intrinsically determined within fetal and adult HSPC, respectively. In order to determine whether fetal and adult HSPC give rise to leukemias with distinct biological properties, we employed a well-characterized viral transduction/transplantation model using activated NOTCH1 (N1ΔE) (Giambra et al., 2015, 2012; Medyouf et al., 2010, 2011; Pear et al., 1996). Briefly, lineage-negative HSPC were sorted with fluorescence-activated cell sorting (FACS) from mouse fetal liver (FL; embryonic day 14.5) and adult BM (8 weeks of age), transduced with N1ΔE lentivirus, and transplanted into lethally irradiated syngeneic C57BL/6 recipient mice (Figure 1A). All recipients of N1ΔE-transduced cells, whether FL or BM in origin, developed primary T cell leukemias with similar penetrance/latency (Figure 1B), immunophenotype (Figure 1C), and disease distribution/burden (data not shown). We then injected primary leukemia cells into secondary and tertiary mouse recipients at limiting dilution in order to assess their serial transplantability. Interestingly, we found that FL leukemias did not transplant efficiently into syngeneic recipients (cell doses up to 1×10^6/recipient; Figure 1D), whereas we and others have generally found BM leukemias to be readily transplantable with measured leukemia-initiating cell (LIC) frequencies of ~1/6,100 cells (95% confidence interval [CI] 1/2,800–13,200 cells) (Giambra et al., 2012). In order to measure and thus compare their respective LIC frequencies more accurately, we performed serial transplantation into more permissive, immunodeficient NOD/Scid/*Il2rg*$^{-/-}$ (NSG) recipients. We found ~1/9 cells from BM leukemias to reproduce disease in NSG recipients (95% CI 1 in 3.3–28 cells), whereas only ~1/4,300 cells from FL leukemias were capable of doing so (95% CI 1/1,500–13,000 cells), or an ~480-fold difference (Figure 1E). Importantly, this difference was consistent even in subsequent tertiary transplants with ~1/11 BM leukemia cells reproducing disease (95% CI 1/4–29 cells) as compared to ~1/1,600 FL leukemia cells (95% CI 1/460–5,800 cells), or an ~150-fold difference (Figure 1F). These transplantation data are summarized in Table S1. The fact that the difference in LIC frequency was manifest in both immunocompetent and immunodeficient recipients suggests that host immunity is not primarily responsible for the poor transplantability of FL leukemias.

In considering other cellular phenotypes that might underlie the difference in transplantability of FL and BM leukemias, we examined cell cycling as induction of cell-cycle entry has been shown to eliminate leukemia stem cells in AML (Saito et al., 2010). Interestingly, we found that FL leukemias tend to cycle more actively than do BM leukemias as measured by Hoechst 33342/Pyronin Y staining (Figure 1G). These findings support the notion that leukemias derived from fetal and adult HSPC have distinct functional programs, and we found the heightened cycling in FL leukemias to be reminiscent of the general proliferative character of fetal as compared to adult HSPC (Pietras et al., 2011).

Pronounced Cycling of NOTCH1-Transduced Fetal HSPC Is Mediated by a Soluble Factor

To explore whether differences between FL and BM leukemias were a reflection of properties inherent in the starting cells from which they were respectively derived, we first assessed cycling activity of HSPC from FL and BM shortly (4 days) after transduction with N1ΔE virus. Similar to established leukemias, transduced (NGFR$^+$) FL cells showed pronounced cycling, whereas transduced BM cells were largely quiescent (Figure 2A; NGFR$^+$ panels on left). Consistent with prior studies, empty virus (EV)-transduced FL cells showed greater cycling activity as compared to their BM counterparts (Pietras et al., 2011); however, N1ΔE virus enhanced cycling of FL cells as compared to EV control, yet had essentially no effect on cycling of BM cells.

Rather unexpectedly, we noticed that non-transduced FL cells in the same cultures as N1ΔE-transduced FL cells also showed enhanced cycling activity (Figure 2A; NGFR$^-$ panels on right), raising the intriguing possibility that N1ΔE-FL cells may express a surface protein or secrete a soluble factor that promotes cycling of neighboring, non-transduced cells. Consistent with this notion, N1ΔE-transduced BM cells showed robust cycling when co-cultured with N1ΔE-FL, but not EV-FL cells (Figure S1A). Next, we added conditioned media from FL cultures to N1ΔE-BM cells in order to determine whether the relevant factors were soluble as opposed to requiring cell-cell contact. Indeed, conditioned media from N1ΔE-FL, but not EV-FL cultures, strongly induced cycling of N1ΔE-BM cells (Figure 2B). Of note, non-transduced BM cells were also induced to cycle by N1ΔE-FL conditioned media, but less so than N1ΔE-BM cells in the same culture, suggesting that activated NOTCH1 may render BM cells more responsive to the N1ΔE-FL-derived soluble factors. We also noted that EV-transduced FL cells cycled more actively than non-transduced cells in the same culture

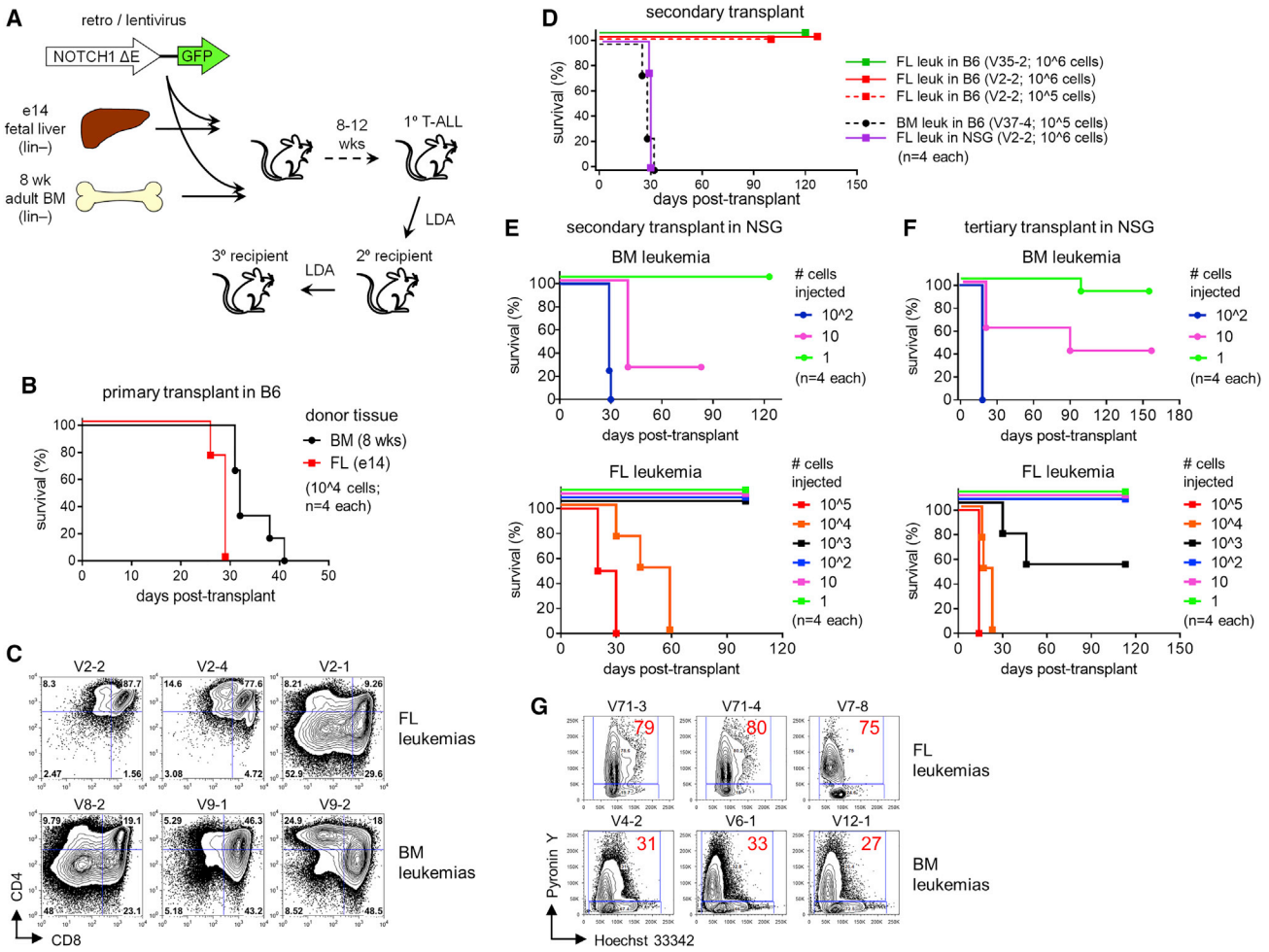

Figure 1. T Cell Leukemias Generated from FL and Adult BM Exhibit Differential Transplantability and Cell Cycling

(A) Schematic of serial transplantation experiments. LDA, limiting dilution analysis.

(B) Survival curves. NOTCH1-ΔE (N1ΔE)-transduced FL and BM cells from C57BL/6 (B6) donors were injected into lethally irradiated, syngeneic B6 primary recipient mice.

(C) Flow cytometric phenotyping. Primary leukemia cells from BM or spleen were harvested from clinically morbid mice. Cells were stained with antibodies against CD4 and CD8 and analyzed by flow cytometry. Gated viable leukemia cells are shown.

(D–F) Survival curves. Primary leukemia cells from (B) were injected into (D) non-irradiated B6 and sublethally irradiated NSG secondary recipient mice and (E) sublethally irradiated NSG secondary recipient mice at limiting dilution. (F) Secondary leukemia cells from (E) were injected into sublethally irradiated NSG tertiary recipient mice at limiting dilution.

(G) G1/G0 cell-cycle analysis. Primary leukemia cells were freshly explanted from clinically morbid animals, stained immediately with Hoechst 33342 and Pyronin Y, and assayed by flow cytometry. Gated live leukemia cells (GFP^+ or $NGFR^+$) are depicted. Three representative animals are shown for each type of leukemia (FL and BM derived).

See also Table S1.

(Figure 2A), which presumably can be attributed to the greater transduction efficiency of actively dividing cells (Park et al., 2000; Sutton et al., 1999).

Auto/Paracrine IGF1 Signaling Is Responsible for Enhanced Cycling in NOTCH1-Transduced Fetal HSPCs

To identify the soluble factor(s) secreted by N1ΔE-FL cells, we performed Affymetrix gene expression profiling of FL and BM-derived HSPC shortly (4 days) after transduction with N1ΔE or EV control. Among a curated list of 1,819 secreted proteins (Meinken et al., 2015), we searched for gene transcripts that were differentially responsive to N1ΔE (as compared to EV controls) in FL versus BM cells. We ranked genes according to the expression (FL N1ΔE – FL EV) – (BM N1ΔE – BM EV), identifying a total of 125 genes with log2 fold change > and false discovery rate (FDR) <0.05 (Table S2). We focused our attention on 40 of those 125 genes whose expression was also significantly altered by N1ΔE in FL cells (log2 fold change >1, FDR <0.05; Figure 2C). We then performed Reactome pathway analysis (Fabregat et al., 2018) and found the top hit and 2 others in the top 15 among 41 identified pathways with FDR <0.05 to relate to IGF signaling (Table S3). We noted with interest *Igf1* as its expression pattern fit well with that of the culture supernatant activity; specifically, *Igf1* was expressed (1) more highly in N1ΔE-transduced FL

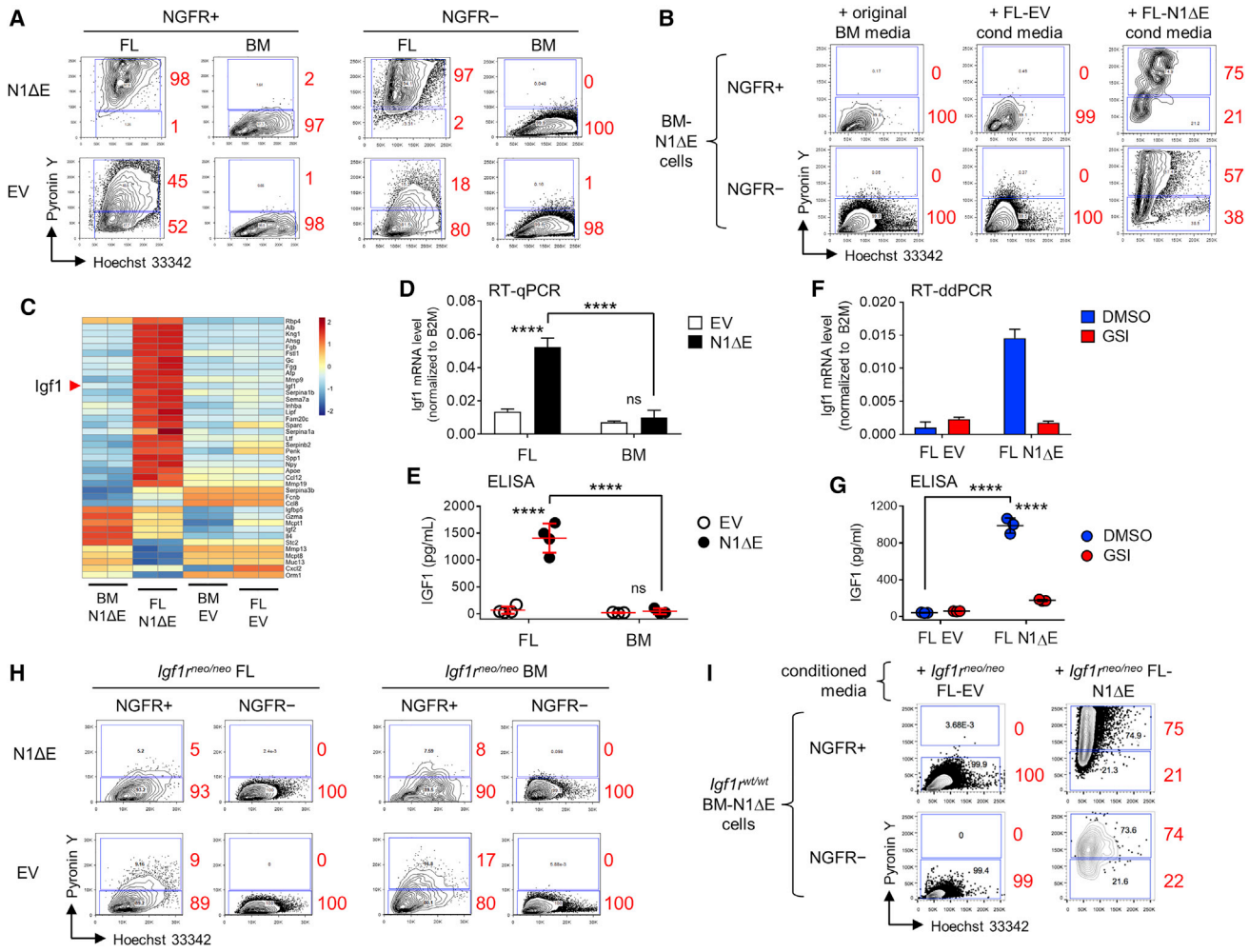

Figure 2. NOTCH1 Induces Autocrine IGF1 Signaling in FL, but Not BM Progenitors

(A, B, H, and I) G1/G0 cell-cycle analysis.

(A and H) Lineage-negative mouse BM and FL progenitors from wild-type (A) or *Igf1r*$^{neo/neo}$ mice (H) were transduced with N1ΔE-NGFR or empty vector (EV) lentivirus and cultured for 4 days prior to staining.

(B and I) BM progenitors from wild-type mice were transduced with N1ΔE-NGFR, while FL progenitors from wild-type (B) or *Igf1r*$^{neo/neo}$ (I) mice were transduced with N1ΔE-NGFR or EV lentivirus. Cells were then cultured for 4 days, after which BM cells were washed and resuspended in conditioned media from FL cultures as indicated. Cells were then cultured for an additional 2 days prior to staining. Gated live NGFR^{+} and NGFR^{-} cells are depicted. Results are representative of multiple replicates.

(C) Heatmap of gene expression array data. BM and FL progenitors were transduced as in (A). RNA was then isolated from transduced cells sorted by FACS and expression profiled. The top 40 differentially expressed genes encoding secreted proteins are depicted. Expression level is scaled by gene with mean = 0 and SD = 1.

(D–G) *Igf1* mRNA and protein expression level.

(D and E) FL and BM progenitors were transduced with N1ΔE or EV lentivirus. Transduced cells were sorted by FACS 4 days later, and RNA was isolated for TaqMan RT-qPCR (D). Transduced cells were sorted by FACS 2 days later and then cultured for an additional 2 days prior to harvest of culture supernatants for ELISA (E). Error bars indicate SD. Assays were performed at least in triplicate.

(F and G) FL progenitors were transduced with N1ΔE or EV lentivirus. Transduced cells were sorted by FACS 4 days later and then cultured for an additional 2 days with γ-secretase inhibitor compound E (GSI, 1 μM final) or DMSO vehicle control. Cells were lysed for RNA and analyzed by TaqMan RT-ddPCR. Error bars indicate 95% CI (F). Culture supernatants were analyzed by ELISA (G). Error bars indicate SD. Data are representative of two replicates. ****$p < 0.0001$; ns, not significant (two-way ANOVA with Tukey's multiple comparisons test).

See also Figures S1 and S2 and Tables S2 and S3.

than BM cells and (2) was induced in FL cells by N1ΔE transduction. We confirmed specific upregulation of *Igf1* by N1ΔE in FL cells at the mRNA level by qRT-PCR (Figure 2D) and also at the protein level by ELISA (Figure 2E). We also showed that upregulation of *Igf1* mRNA and protein in N1ΔE-FL cells was reversed by subsequent treatment with compound E, a potent NOTCH signaling/γ-secretase inhibitor (Figures 2F and 2G), suggesting that N1ΔE may be acting directly to upregulate *Igf1* transcription. Notably, addition of recombinant IGF1 to N1ΔE-BM cultures induced cell cycling (Figure S1B), thus phenocopying

the effect of N1ΔE-FL conditioned media. The response to IGF1 was more pronounced in N1ΔE-transduced cells ($NGFR^+$) as compared to non-transduced cells ($NGFR^-$) in the same culture, similar to the response of N1ΔE-BM cells to N1ΔE-FL conditioned media (Figure 2B). These results reveal that IGF1 is a plausible candidate but do not firmly establish that it is in fact the relevant soluble factor, underlying the cycling phenotype.

To address whether IGF1 was indeed the relevant factor in our system, we utilized *Igf1r*$^{neo/neo}$ mice, which express markedly reduced amounts of IGF1R due to a retained *neo* cassette in the 2nd intron that leads to altered splicing (Holzenberger et al., 2000; Medyouf et al., 2011). In striking contrast to wild-type cells, FL HSPC from *Igf1r*$^{neo/neo}$ mice fail to cycle in response to N1ΔE (Figure 2H), yet yield conditioned supernatants that induce cycling of *Igf1r*$^{wt/wt}$ BM cells (Figure 2I). These data are consistent with the interpretation that *Igf1r*$^{neo/neo}$ cells secrete but cannot themselves respond to the relevant soluble activity, which we would thus conclude to be IGF1. We also confirmed that N1ΔE induces *Igf1r*$^{neo/neo}$ FL cells to express *Igf1* mRNA (Figure S1C). Taken together, these data support the conclusion that activated NOTCH1 drives cell cycling in fetal, but not adult HSPC, and that this effect is mediated largely through auto/paracrine IGF1 signaling.

One important variable introduced by transduction with N1ΔE is that activated NOTCH1 promotes differentiation toward T lymphoid cell fate (Pear and Radtke, 2003), whereas EV controls are more likely to adopt myeloid cell fates under the *in vitro* culture conditions utilized. Within the 4-day culture period following HSPC transduction, N1ΔE did modestly impede acquisition of myeloid lineage markers Mac1 and Gr1 as compared to EV controls but did not appreciably promote acquisition of the early T lineage marker Thy1 (Figure S2A). Nonetheless, we also sorted using FACS the $Mac1^-$ $Gr1^-$ subset from these cultures and confirmed significant upregulation of *Igf1* mRNA by N1ΔE in FL, but not BM cells (Figure S2B), thus arguing against the possibility that differences in *Igf1* mRNA levels between EV and N1ΔE-transduced cells are secondary to cell differentiation.

Chromatin Structure over the *Igf1* Promoter Is Permissive to NOTCH1 in FL, but Not BM Cells

The ability of NOTCH1 to induce *Igf1* in FL, but not BM cells led us to hypothesize that NOTCH1/CSL transcriptional complexes may have access to and load at the *Igf1* locus in FL, but not BM cells. In fact, local chromatin immunoprecipitation (ChIP) assay with anti-NOTCH1 antibody revealed substantial enrichment of the *Igf1* promoter region containing 3 canonical CSL binding sites (TGGGAA) (Del Bianco et al., 2010) in N1ΔE-FL cells, but not in N1ΔE-BM cells (Figures 3A and 3B). To explore potential reasons why NOTCH1/CSL complexes were not loading at the *Igf1* promoter in N1ΔE-BM cells, we examined histone modification marks by local ChIP using a series of 7 primer sets spanning the two *Igf1* promoters, P1 and P2, located immediately upstream of exons 1 and 2, respectively (LeRoith and Roberts, 1991). We examined both FL and BM cells transduced by N1ΔE virus as well as by EV control. We found that P1 and P2 were significantly more enriched for H3K4me3 (associated with active gene promoters) in FL cells transduced by N1ΔE as compared to EV controls, while P1 and P2 were similarly, but less robustly marked by H3K4me3 in N1ΔE-BM cells as compared to EV-BM cells (Figure 3C). Interestingly, there was significantly more enrichment over P1 and P2 for H3K27me3 (associated with inactive genes) in N1ΔE-BM as compared to N1ΔE-FL cells (Figure 3D), consistent with the notion that local chromatin is less permissive to gene expression in N1ΔE-BM than N1ΔE-FL cells. Subsequent ChIP sequencing (ChIP-seq) analyses also confirmed greater H3K27me3 density (i.e., broader region of MACS2 peak calls) over the *Igf1* promoter region in N1ΔE-BM as compared to N1ΔE-FL cells (Figure 3E). These chromatin features would suggest that the *Igf1* promoter can be regarded as active in N1ΔE-FL cells, and inactive but primed or "poised" in N1ΔE-BM cells. These findings support that NOTCH1 loads more effectively at the *Igf1* promoter in FL than BM cells, and that the presence of repressive, H3K27me3-modified chromatin over this region in BM cells may be responsible for limiting access/loading by NOTCH1. Of note, EV-transduced BM cells also showed somewhat greater enrichment for H3K27me3 than EV-FL cells, supporting that the *Igf1* locus is less accessible "at baseline" in BM than FL cells.

EZH2 Restricts Access to the *Igf1* Promoter Region in BM Cells

The developmental switch from fetal to adult program hematopoiesis has been studied by several groups (Bowie et al., 2007; Copley et al., 2013; Kim et al., 2007), and it was recently shown that EZH2, an H3K27 methyltransferase (Lund et al., 2014), contributes to this process by repressing the *Lin28b/let-7* pathway in adult mouse BM HSPC (Oshima et al., 2016). This led us to question whether EZH2 might be responsible for BM-specific repression of the *Igf1* promoter in our system. In fact, we found greater levels of *Ezh2* mRNA in BM than FL cells, and this difference was more pronounced in N1ΔE than EV-transduced cells (Figure 4A). We then knocked down EZH2 in N1ΔE-BM cells using lentiviral short hairpin RNAs (shRNAs) (Figure S3) and found this to result in increased *Igf1* expression at the level of both mRNA and secreted protein (Figures 4B and 4C), and also to enhance cell cycling (Figure 4D). We further confirmed this effect using a small molecule inhibitor of EZH2/1 histone lysine methyltransferase activity, UNC1999 (Konze et al., 2013), which led to increased *Igf1* mRNA and protein expression as compared to UNC2400, a close chemical analog with >1,000-fold lower potency (Figures 4E and 4F).

EZH2 Suppresses *Igf1* in BM-Derived Leukemias by Preventing Promoter Access by NOTCH1

We next sought to confirm whether EZH2 was responsible for repression of *Igf1* in BM cells after progression to leukemic disease. Indeed, knockdown of EZH2 in established BM leukemias resulted in increased *Igf1* mRNA and protein (Figures 5A and 5B), and increased cell cycling (Figure 5C). We also treated BM leukemias with UNC1999 to inhibit EZH2 activity and found this resulted in increased *Igf1* mRNA and protein. This effect was abrogated by co-treatment with a NOTCH signaling/γ-secretase inhibitor (Figures 5D and 5E), thus confirming that *Igf1* expression is NOTCH-dependent in this context.

The results up to this point suggest that EZH2 restricts *Igf1* expression by catalyzing H3K27 trimethylation at the *Igf1* promoter, thereby preventing NOTCH1 from binding. To test this notion further, we treated BM leukemias with UNC1999 to see

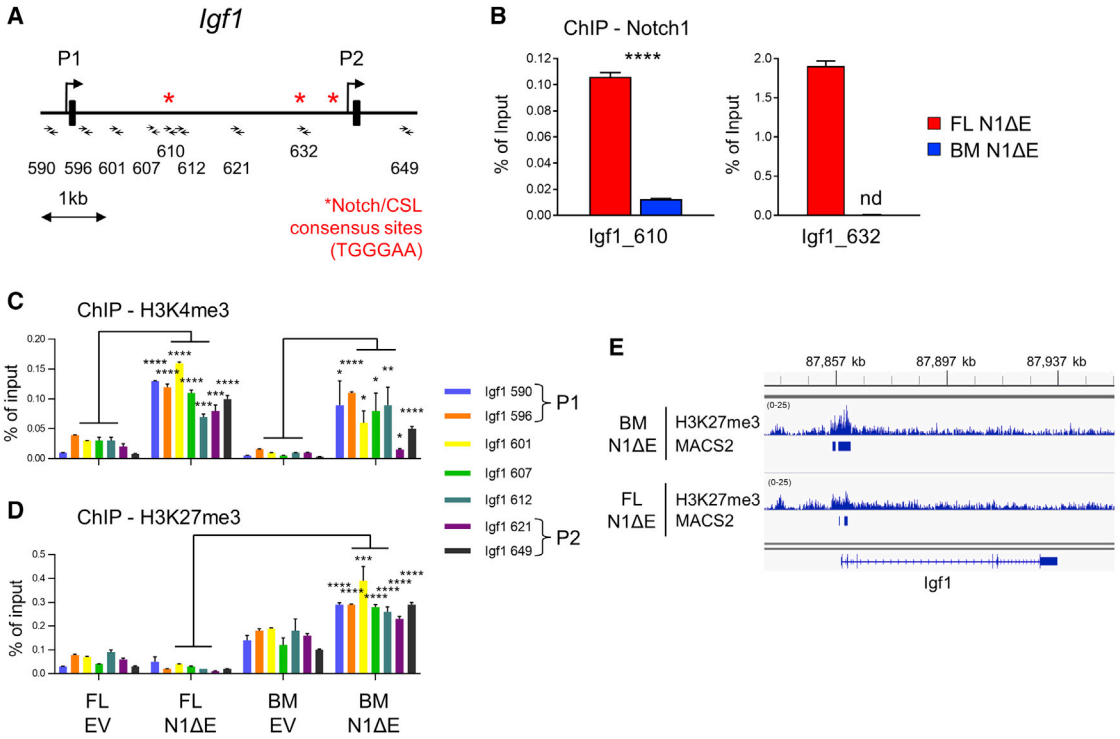

Figure 3. H3K27 Trimethylation over the *Igf1* Promoter in Adult Cells Correlates with Restricted Access by NOTCH1

(A) Mouse *Igf1* promoter region. Promoters P1 and P2 are shown, along with putative NOTCH/CSL consensus binding sites. Primer pairs used for ChIP-qPCR assays are indicated by small arrows. Map positions *xyz* correspond to locus coordinates chr10:87,8xy,z00 (GRCm38).

(B–D) ChIP-qPCR analysis. FL and BM progenitors were transduced with N1ΔE or EV lentivirus and cultured for 3 days. Transduced cells were then sorted by FACS and fixed for ChIP assay. ChIP was performed with antibodies against NOTCH1 (B), H3K4me3 (C), H3K27me3, or immunoglobulin G (IgG) control (D). Primers pairs spanning the *Igf1* P1/P2 promoter region as indicated in (A) were used for qPCR on immunoprecipitated DNA. Values are expressed as a fraction of input DNA controls. Values for IgG controls were negligible/below the limit of detection for the assay (data not shown). Mean values are plotted for assays performed in triplicate Error bars indicate SD. nd, not detected; *$p < 0.05$; **$p < 0.01$; ***$p < 0.001$; ****$p < 0.0001$ (Student's t test).

(E) ChIP-seq analysis. FL and BM progenitors were transduced, sorted, and fixed as in (B)–(D). ChIP-seq was performed with an anti-H3K27me3 antibody. Aligned reads over the mouse *Igf1* locus are shown along with MACS2 peak calls. Background correction was applied based on signals from input DNA libraries constructed in parallel.

See also Table S7.

whether reversal of H3K27me3 marks would then allow NOTCH1 to bind at the *Igf1* promoter. Indeed, UNC1999 treatment led to reduced H3K27me3 levels and increased NOTCH1 occupancy at the *Igf1* promoter as compared to UNC2400 controls (Figure 5F). Taken together, these results support the idea that EZH2 places H3K27me3 marks over the *Igf1* promoter, thus configuring local chromatin into a less accessible state and limiting the ability of NOTCH1 to load and stimulate *Igf1* transcription.

EZH2 Restricts *IGF1* Promoter Access by NOTCH1 in Human Leukemia Cells

To ascertain the relevance of these findings to human disease, we first examined publicly available Affymetrix gene expression microarray data from two large T-ALL cohorts totaling 228 patient samples (Homminga et al., 2011; Piovan et al., 2013). We found *EZH2* and *IGF1* mRNA levels were significantly inversely correlated in each of the two cohorts (Figure S4A). To test this correlation further, we examined a pair of human T-ALL cell lines, CUTLL1 and HPBALL, which exhibit active NOTCH1 signaling (Palomero et al., 2006; Weng et al., 2004) and express EZH2 protein at readily detectable levels. Consistent with findings in mouse cells, we observed that shRNA-mediated knockdown (Figure S3) or enzymatic inhibition of EZH2 with UNC1999 resulted in increased expression of *IGF1* mRNA (Figures 6A and 6C). Importantly, we confirmed that knockdown or inhibition of EZH2 resulted in reduced H3K27me3 levels and increased NOTCH1 protein occupancy at the *IGF1* promoter (Figures 6B, 6D, and S4B). Of note, analysis of a previously published ChIP-seq dataset (Wang et al., 2014) revealed that NOTCH1/CSL complexes occupy a discrete site near the *IGF1* promoter in CUTLL1 cells (Figure S4C). Indeed, addition of γ-secretase inhibitor blocked *IGF1* mRNA induction by UNC1999 (Figure 6C), further supporting that NOTCH1 activates *IGF1* transcription directly by physical loading at its promoter. Similar results were obtained with the HPBALL cell line (data not shown). Collectively, these results support that EHZ2 controls access to the *IGF1* promoter by NOTCH1 in human T-ALL as it does in mouse BM and mouse BM-derived leukemias.

We additionally tested whether the EZH2/NOTCH1/IGF1 axis was similarly operative in $CD34^+$ human cord blood (CB) progenitors that had been transduced first with LMO2 and

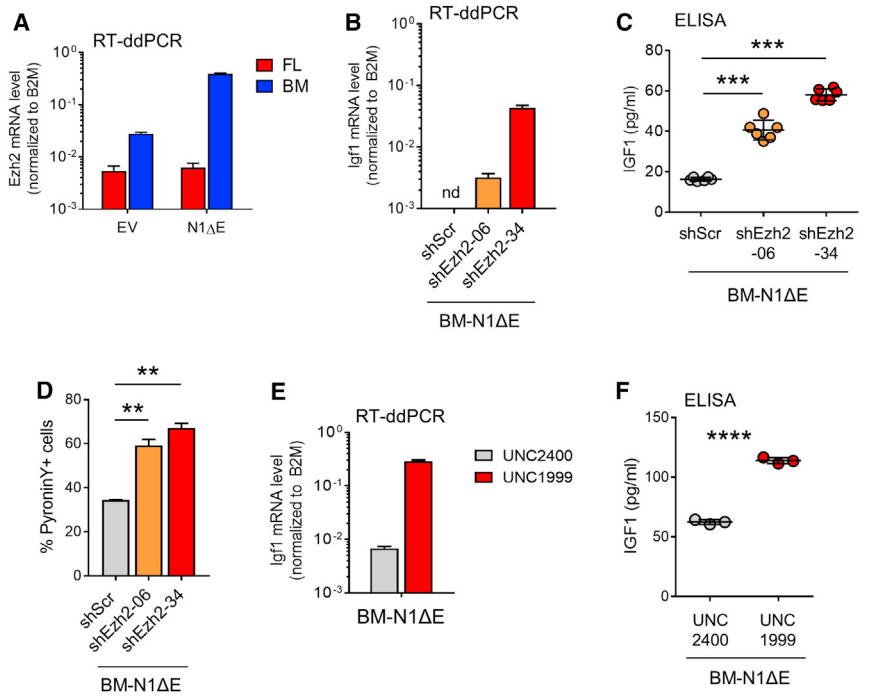

Figure 4. Knockdown or Inhibition of EZH2 Activates *Igf1* Expression in N1ΔE-Transduced BM Cells

(A) *Ezh2* mRNA expression level. FL and BM progenitors were transduced with N1ΔE or EV lentivirus and cultured for 4 days. RNA was then isolated from sorted transduced cells sorted by FACS and analyzed by TaqMan RT-droplet digital PCR (RT-ddPCR).

(B and C) *Igf1* mRNA and protein expression level. BM progenitors were transduced with N1ΔE-GFP and shEzh2- or scrambled control (shScr)-NGFR lentiviruses on successive days and then cultured for 4 days. Doubly transduced (GFP^+ $NGFR^+$) cells were then sorted by FACS and cultured for an additional 3 days prior to harvest. Cells were lysed for RNA and analyzed by TaqMan RT-ddPCR (B). Culture supernatants were analyzed by ELISA (C).

(D) G1/G0 cell-cycle analysis. BM progenitors were transduced with N1ΔE-GFP and shEzh2- or shScr-NGFR lentiviruses on successive days and then cultured for 4 days. Cells were then stained with Hoechst/Pyronin and assayed by flow cytometry with gating for live, GFP^+ $NGFR^+$ cells.

(E and F) *Igf1* mRNA and protein expression level. BM progenitors were transduced with N1ΔE lentivirus and cultured for 2 days. Transduced cells were then sorted by FACS, treated with either the EZH2/1 inhibitor UNC1999 or UNC2400 control at 2 μM, and cultured for an additional 3 days. Cells were lysed for RNA and analyzed by TaqMan RT-ddPCR) (E). Culture supernatants were analyzed by ELISA (F). Error bars in (A), (B), and (E) represent 95% CI; in (C), (D), and (F), they represent SD. Data shown are representative of at least two replicates. nd, not detected; $^{**}p < 0.01$; $^{***}p < 0.001$; $^{****}p < 0.0001$ (Student's t test).

See also Figure S3.

TAL1 (to mimic enforced expression as occurs with recurrent TCR-LMO2/TAL1 gene rearrangements) and then with activated NOTCH1 (Figure 6E), which may be regarded to simulate the stepwise acquisition of oncogenic hits in human T-ALL (De Bie et al., 2018). Consistent with results in human T-ALL cell lines, inhibition of EZH2 with UNC1999 resulted in NOTCH-dependent activation of *IGF1* mRNA expression (Figure 6F). Of note, CB cells transduced with this combination (LMO2+TAL1+NOTCH1) expand robustly *in vitro* and, when combined additionally with BMI1, produce aggressive, serially transplantable T-ALL *in vivo* with short latency (M. Kusakabe, A. Sun, K.T., et al., unpublished data).

Enforced IGF1 Signaling Limits Leukemia-Initiating Activity

Our earlier observation that FL-derived leukemias with robust autocrine IGF1 signaling showed lower LIC activity as compared to BM-derived leukemias suggested the possibility that IGF1 signaling may drive cells into cycle and thereby deplete the LIC compartment. To test this idea, we transduced mouse BM-derived leukemias and human patient-derived xenograft (PDX) leukemias with constitutively activated IGF1R (CA) lentivirus prior to transplantation into recipient mice. We included both empty vector (EV) and a kinase dead mutant construct (K1003A; CAKD) as negative controls. While 23/24 animals receiving EV- or CAKD-transduced mouse BM leukemia cells died within 22 days, 11/12 animals receiving CA-transduced cells showed no evidence of disease up to 92 days post-transplant (Figure 7A, Table S4).

In similar experiments with human PDX leukemias (Table S5), most recipients developed morbid disease regardless of being transduced with EV, CA, or CAKD; however, at necropsy we found that tumors in 12/13 animals from the CA group were largely devoid of the CA construct (>85% of cells were $NGFR^-$), consistent with outgrowth of non-transduced cells in the recipient (Table S4). In contrast, tumors in 11/13 animals from the CAKD group retained >90% $NGFR^+$ cells. By scoring only tumors that had retained the original construct as "disease-specific" deaths, censoring tumors that had lost the original construct, and, ignoring those not assessed for NGFR content, we arrived at the conclusion that transduction with the CA construct significantly impairs LIC activity in human PDXs as compared to CAKD controls (Figure 7B).

We also tested the effect of co-mingling of mouse BM- and FL-derived leukemia cells on transplantability of the BM leukemia cells. After co-culture of BM and FL leukemia cells in the same culture well for 4 days, BM leukemia cells showed reduced LIC activity as compared to control (not co-mingled) cells (Figure S5). Moreover, direct treatment of primary mouse BM and human PDX leukemia cells with IGF1 *in vitro*, followed thereafter by transplantation into secondary recipients also resulted in reduction of LIC activity (Figure 7C; Table S6). Overall, these data support the notion that enforced IGF1 signaling, either by genetic or pharmacologic means, can limit LIC activity in T-ALL, presumably by drawing otherwise quiescent leukemia stem cells into cycle.

One issue to consider is whether the extent of *IGF1* activation necessary to restrict LIC activity represents "supraphysiologic" levels in excess of that which is or can be achieved through

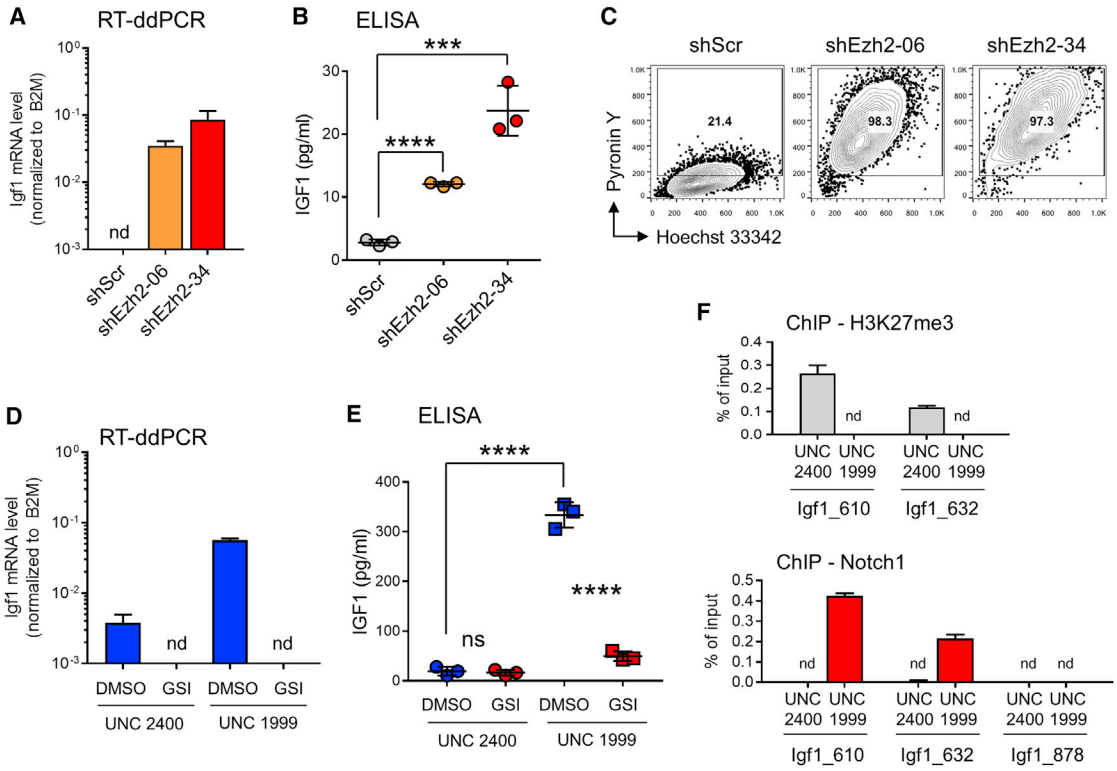

Figure 5. EZH2 Represses *Igf1* in BM Leukemias by Restricting Promoter Access by NOTCH1

(A, B, D, and E) *Igf1* mRNA and protein expression level.

(A and B) BM leukemia cells were transduced with shEzh2- or shScr-NGFR lentivirus and cultured for 4 days. Transduced cells were then sorted by FACS and cultured for an additional 3 days prior to harvest.

(D and E) BM leukemia cells were treated with the EZH2 inhibitor UNC1999 or UNC2400 control (2 μM final) in combination with GSI (1 μM final) or DMSO control for 2 days.

(A and D) Cells were lysed for RNA and analyzed by TaqMan RT-ddPCR.

(B and E) Culture supernatants were analyzed by ELISA.

(C) G1/G0 cell-cycle analysis. BM leukemia cells were transduced as in (A) and (B). Cells were stained and analyzed 4 days later. Live, gated $NGFR^+$ leukemia cells are depicted.

(F) ChIP-ddPCR analysis. BM leukemia cells were cultured with either UNC1999 or UNC2400 (2 μM final) for 3 days prior to fixation. ChIP was performed with antibodies against H3K27me3, NOTCH1, or IgG control. Primers flanking NOTCH/CSL binding sites in the *Igf1* P1/P2 promoter region (*Igf1*_610 and *Igf1*_632) or a downstream control region (*Igf1*_878) were used for ddPCR on immunoprecipitated DNA. Values are expressed as a fraction of input DNA controls. Values for IgG controls were negligible/below the limit of detection for the assay (data not shown).

Error bars in (A), (D), and (F) represent 95% CI; in (B) and (E), they represent SD. Data shown are representative of two independent BM leukemias. nd, not detected; ns, not significant; ***$p < 0.001$; ****$p < 0.0001$ (B, Student's t test; E, two-way ANOVA with Tukey's multiple comparisons test).

See also Figure S3 and Table S7.

the NOTCH1:*IGF1* axis. To address this point, we examined NOTCH1 protein occupancy levels over the *IGF1* promoter region by ChIP in each of the 3 human PDX models. We found that, while NOTCH1 protein was detectable to varying extents at the *IGF1* promoter, treatment with UNC1999 consistently resulted in increased NOTCH1 occupancy, along with decreased H3K27me3 and increased *IGF1* mRNA levels, the latter of which was abrogated by NOTCH1 inhibition with γ-secretase inhibitor (Figure S6). It is difficult to determine precisely how levels of IGF1 signaling attained by EZH2 inhibition compare to those attained by IGF1R-CA transduction or IGF1 treatment; however, it may be desirable from a therapeutic perspective to exceed into supraphysiologic levels of IGF1 signaling in order to achieve the greatest depth of LIC depletion, assuming of course the side effect profile can be managed clinically.

Since our data would suggest that EZH2 inhibition could be used to induce auto/paracrine IGF1 signaling among human T-ALL cells, we tested whether UNC1999-treated cells would also show reduced LIC activity. Indeed, human PDX cells treated with UNC1999 *in vitro* and then injected immediately thereafter into NSG mice showed significantly lower levels of peripheral blood engraftment 58 days later and prolonged survival of recipient mice, as compared to the inactive UNC2400 control (Figure S7). Although further *in vivo* drug studies are needed to validate this result, our findings suggest that potentiating IGF1 signaling through inhibition of EZH2 could contribute to existing therapeutic regimens in human T-ALL under circumstances in which other, IGF1-independent or potentially pro-oncogenic effects of EZH2 inhibition can be balanced or otherwise mitigated.

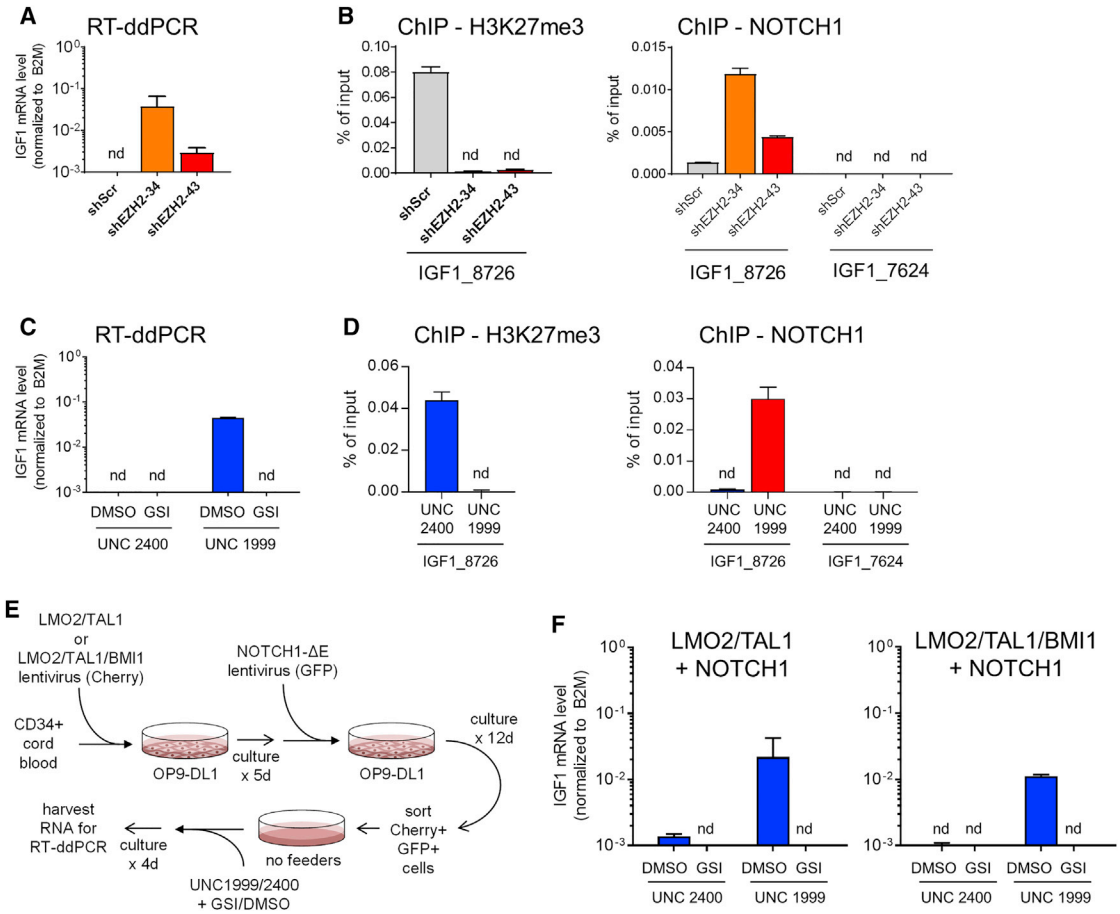

Figure 6. EZH2 Represses *IGF1* in Human T-ALL by Restricting Promoter access by NOTCH1

(A and B) The human T-ALL cell line CUTLL1 was transduced with shEZH2- or shScr-NGFR lentivirus and cultured for 4 days. Transduced (NGFR$^+$) cells were then sorted by FACS and either lysed for RNA or fixed for ChIP assay.

(C and D) CUTLL1 cells were cultured for 2 days with (C) the EZH2 inhibitor UNC1999 or UNC2400 control (2 μM final) in combination with GSI (1 μM final) or DMSO control (C), or UNC1999/2400 only (D). Cells were then either lysed for RNA for fixed for ChIP assay.

(A and C) *IGF1* mRNA expression level by TaqMan RT-ddPCR.

(B and D) ChIP-ddPCR analysis. ChIP was performed with antibodies against H3K27me3, NOTCH1, or IgG control. Primer pairs near (IGF1_8726) or distant from (IGF1_7624) the NOTCH1/CSL binding site in the *IGF1* P1/P2 promoter region (see Figure S7) were used for ddPCR on immunoprecipitated DNA. Values are expressed as a fraction of input DNA controls. Values for IgG controls were negligible/below the limit of detection for the assay (data not shown).

(E and F) CD34$^+$ CB progenitors were transduced with lentivirus encoding LMO2/TAL1 or LMO2/TAL1/BMI1 (Cherry) and then cultured on OP9-DL1 feeders for 5 days. Cells were subsequently transduced with lentivirus encoding activated NOTCH1–ΔE (GFP) and cultured for an additional 12 days. Doubly transduced (Cherry$^+$ GFP$^+$) cells were sorted with FACS and then cultured without feeders in the presence of EZH2 inhibitor UNC1999 or UNC2400 control (2 μM final) in combination with GSI (1 μM final) or DMSO control for 2 days. RNA was then harvested and analyzed by TaqMan RT-ddPCR. Transductions were performed in triplicate. Schematic of experiment (E). *IGF1* mRNA expression level (F).

Error bars represent 95% CI. nd, not detected.

See also Figures S3 and S4 and Table S7.

DISCUSSION

In our efforts to explore the effect of aging on leukemia cells of origin, we revealed a fetal-specific autocrine IGF1 pathway that is augmented by NOTCH1 signaling and restricted in adult cells by the epigenetic modifier *Ezh2*. In reversing H3K27 trimethylation of the *Igf1* promoter by knockdown or enzymatic inhibition of EZH2, we were able to re-engage autocrine IGF1 signaling in adult cells. Further, we were able to demonstrate that reversal of H3K27 trimethylation also led to increased NOTCH1 occupancy at the *Igf1*/*IGF1* promoter in both mouse and human leukemia cells, supporting the idea that the H3K27me3 modification impedes transcription factor access to DNA, as was shown recently in differentiating embryonic stem cells (ESCs) (Petruk et al., 2017).

Recent studies have demonstrated changes in the composition and potentiality among HSPC populations, which occur as part of a preset developmental program, are mediated at least in part by epigenetic modifications (Notta et al., 2016; Yu et al., 2016). As well, in both mouse and *de novo*, or "synthetic," human models of *MLL-AF9*-induced AML, there is evidence that distinct genetic programming of fetal versus adult hematopoietic progenitor cells can dictate differential phenotypes in leukemias

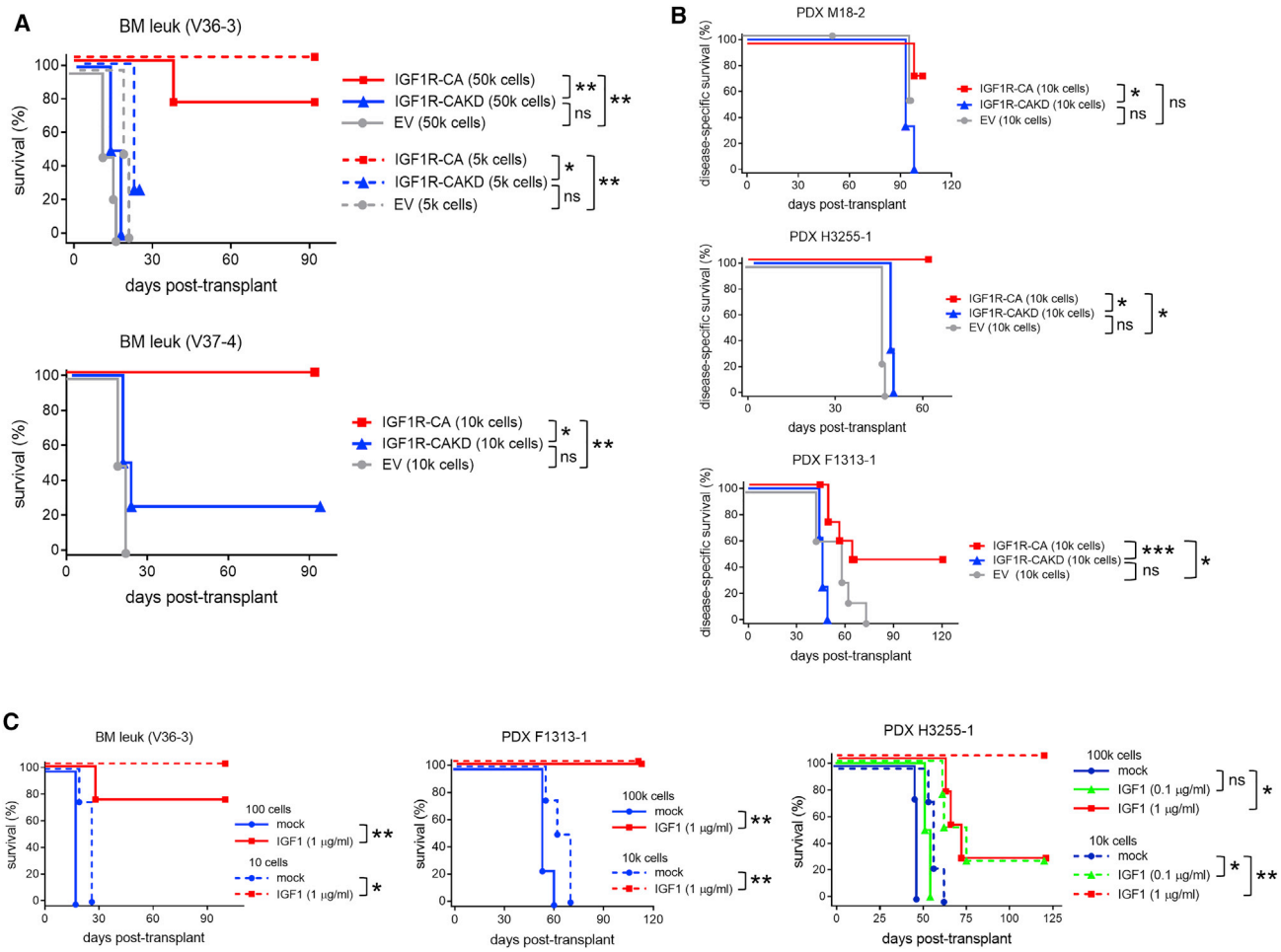

Figure 7. Enforced IGF1 Signaling Limits Leukemia-Initiating Activity in Mouse BM Leukemias and Human T-ALL

(A–B) Survival curves. Primary mouse BM leukemias (A) or human PDX T-ALLs (B) were transduced with lentiviruses encoding constitutively active IGF1R (IGF1R-CA), a kinase dead mutant (IGF1R-CAKD), or EV control and cultured for 3 days. Transduced (NGFR$^+$) cells were then sorted with FACS and transplanted into syngeneic (A) or immunodeficient (B) NSG recipient mice, respectively, at the indicated cell doses.

(C) Mouse BM or human PDX leukemias were cultured with or without supplemental recombinant IGF1 for 2 days. Viable leukemia cells were then sorted with FACS and injected into NSG recipient mice at the indicated cell doses.

ns, not significant; *$p < 0.05$; **$p < 0.01$; ***$p < 0.001$ (log-rank test).

See also Figures S5–S7 and Tables S4–S6.

that arise from these cells (Chen et al., 2011; Horton et al., 2013; Man et al., 2016). We have demonstrated here epigenetic regulation of aging-related changes in hematopoietic progenitors that alters both the gene expression and resulting biological behavior of derived mouse T cell leukemias. These findings support and extend upon an evolving paradigm for aging-dependent features in mouse leukemia cells of origin and have led us to the prediction that activation of IGF1 signaling may represent a targetable aspect of human T-ALL biology.

Our observation that FL leukemias exhibit 2-log lower LIC activity as compared to BM leukemias led us to consider that invoking fetal-like programs in BM leukemias might reduce their leukemia stem cell content. Indeed, we found that enforced IGF1 signaling in mouse T-ALL and human PDX tumors limited their ability to propagate disease in secondary recipients. Of note, treatment of primary human AML with G-CSF can indeed draw leukemia stem cells into cycle, rendering them more sensitive to conventional chemotherapy and improving survival of xenografted recipient mice (Saito et al., 2010). Further, growth factor stimulation or "priming" in combination with chemotherapy has shown clinical benefit in some, but not all human AML contexts (Löwenberg et al., 2003; Pabst et al., 2012). This approach remains controversial and any potential clinical benefit would likely be limited to particular clinical scenarios, perhaps such as drawing minimal residual disease (MRD) cells into cycle in anticipation of subsequent rounds of consolidation chemotherapy.

Most mouse T-ALL models are framed within the context of adult hematopoietic cells, and thus the effect of starting from different developmental stages has not previously been explored in this disease context, and only to a limited extent in other contexts (i.e., *MLL-AF9* in AML) (Park, 2016). For instance, adult donors are generally utilized for BM transplantation experiments

(Chiang et al., 2013; Herranz et al., 2015; Medyouf et al., 2010; Ntziachristos et al., 2014; Pear et al., 1996; Wendorff et al., 2010), while transgenic models typically have relatively lengthy latencies such that one might presume that critical transforming events have taken place after cells have traversed the fetal-to-adult switch point (De Keersmaecker et al., 2010; Draheim et al., 2011; Tremblay et al., 2010). By starting with E14.5 FL HSPC in our studies and achieving frank leukemias within 4 weeks, we presume that critical cellular transformation events had occurred prior to the fetal-to-adult switch (Bowie et al., 2007).

It is of interest that Ntziachristos et al. (2014) presented data supporting that NOTCH1 could "evict" PRC2/EZH2 complexes from promoters of its target genes including *Hes1*, *Dtx1*, *Ptcra*, and *Myc*, thereby reducing local H3K27me3 and facilitating transcription. This discrepancy with our findings has multiple possible explanations. First, *Igf1* was not among the genes they had identified as showing decreased H3K27me3/increased mRNA in mouse NOTCH1 T-ALL cells (as compared to normal DP thymocytes), which may suggest that *Igf1* resides within a class of NOTCH1 target genes that is regulated differently than *Hes1*, *Dtx1*, etc. Second, it may be that NOTCH1 can accomplish only partial eviction of PRC2 from the *Igf1* promoter in BM cells, with additional EZH2 antagonism required to open the locus more fully to transcriptional activation. Of note, increased cell growth driven by auto/paracrine IGF1 signaling would presumably also favor accumulation/propagation of loss-of-function *EZH2* mutations, at least within transit-amplifying cells, which constitute the bulk of a tumor cell population.

When we first conceived these studies, we anticipated that perhaps mouse FL leukemias might resemble human pediatric leukemias, while mouse BM leukemias might resemble human adult leukemias. The switch from fetal to adult hematopoiesis in humans, however, likely occurs shortly after birth and certainly much earlier than the conventional cutoff between pediatric and adult patients (16–18 years). With this in mind, one might expect that a fetal-like condition would likely be recapitulated only in neonatal or infant leukemias; however, the vast majority of these are AML or B-ALL involving *MLL* rearrangements (Felix and Lange, 1999), with neonatal/infant cases of T-ALL being exceedingly rare. We would thus surmise that pediatric T-ALL as a group encompasses mostly, if not exclusively "adult" rather than "fetal" pattern disease. The regulatory pathway involving EZH2, NOTCH1, and IGF1 revealed here could nonetheless serve as a targetable aspect of T-ALL biology in situations, pediatric or adult, where IGF1 signaling is limited. Of note, we reported in a prior study that inhibition of IGF1 signaling compromised LIC activity in T-ALL (Medyouf et al., 2011). We reconcile that study with our current findings by positing that "adult" program LICs require a moderate amount of IGF1 signaling to maintain homeostasis, but auto/paracrine IGF1 secretion contributes an additional layer of stimulation that leads to LIC depletion/exhaustion. Our work also illustrates that the study of age-related genetic/epigenetic programs can provide insight into disease biology and suggest novel therapeutic approaches.

STAR★METHODS

Detailed methods are provided in the online version of this paper and include the following:

SUPPLEMENTAL INFORMATION

Supplemental Information includes seven figures and seven tables and can be found with this article online at https://doi.org/10.1016/j.stem.2018.08.018.

ACKNOWLEDGMENTS

This work was supported by operating and program project grants from the Canadian Institutes of Health Research (CIHR) and Terry Fox Research Institute (TFRI), respectively, to A.P.W. V.G. received fellowship support from the Michael Smith Foundation for Health Research (MSFHR) and grants from the Fondazione con il SUD ("Brain2South") and the Italian Association for Research on Cancer ("My First AIRC Grant").

AUTHOR CONTRIBUTIONS

V.G. and A.P.W. designed experiments; V.G., S.G., D.G., R.S., S.H.L., P.P., C.E.J., and A.L. generated the data; K.T., C.H., A.L., and A.C. analyzed informatics data; V.G. and A.P.W. interpreted results and wrote the manuscript; and M.H. and C.J.E. provided advice and discussion.

DECLARATION OF INTERESTS

The authors declare no competing interests.

Received: October 27, 2017
Revised: June 15, 2018
Accepted: August 30, 2018
Published: September 27, 2018

REFERENCES

Alizadeh, A.A., Eisen, M.B., Davis, R.E., Ma, C., Lossos, I.S., Rosenwald, A., Boldrick, J.C., Sabet, H., Tran, T., Yu, X., et al. (2000). Distinct types of diffuse large B-cell lymphoma identified by gene expression profiling. Nature *403*, 503–511.

Armstrong, F., Brunet de la Grange, P., Gerby, B., Rouyez, M.C., Calvo, J., Fontenay, M., Boissel, N., Dombret, H., Baruchel, A., Landman-Parker, J., et al. (2009). NOTCH is a key regulator of human T-cell acute leukemia initiating cell activity. Blood *113*, 1730–1740.

Babovic, S., and Eaves, C.J. (2014). Hierarchical organization of fetal and adult hematopoietic stem cells. Exp. Cell Res. *329*, 185–191.

Bowie, M.B., Kent, D.G., Dykstra, B., McKnight, K.D., McCaffrey, L., Hoodless, P.A., and Eaves, C.J. (2007). Identification of a new intrinsically timed developmental checkpoint that reprograms key hematopoietic stem cell properties. Proc. Natl. Acad. Sci. USA *104*, 5878–5882.

Chen, W., O'Sullivan, M.G., Hudson, W., and Kersey, J. (2011). Modeling human infant MLL leukemia in mice: Leukemia from fetal liver differs from that originating in postnatal marrow. Blood *117*, 3474–3475.

Chiang, M.Y., Shestova, O., Xu, L., Aster, J.C., and Pear, W.S. (2013). Divergent effects of supraphysiologic Notch signals on leukemia stem cells and hematopoietic stem cells. Blood *121*, 905–917.

Copley, M.R., Babovic, S., Benz, C., Knapp, D.J.H.F., Beer, P.A., Kent, D.G., Wohrer, S., Treloar, D.Q., Day, C., Rowe, K., et al. (2013). The Lin28b-let-7-Hmga2 axis determines the higher self-renewal potential of fetal haematopoietic stem cells. Nat. Cell Biol. *15*, 916–925.

Coustan-Smith, E., Mullighan, C.G., Onciu, M., Behm, F.G., Raimondi, S.C., Pei, D., Cheng, C., Su, X., Rubnitz, J.E., Basso, G., et al. (2009). Early T-cell precursor leukaemia: A subtype of very high-risk acute lymphoblastic leukaemia. Lancet Oncol. *10*, 147–156.

Dai, M., Wang, P., Boyd, A.D., Kostov, G., Athey, B., Jones, E.G., Bunney, W.E., Myers, R.M., Speed, T.P., Akil, H., et al. (2005). Evolving gene/transcript definitions significantly alter the interpretation of GeneChip data. Nucleic Acids Res. *33*, e175.

De Bie, J., Demeyer, S., Alberti-Servera, L., Geerdens, E., Segers, H., Broux, M., De Keersmaecker, K., Michaux, L., Vandenberghe, P., Voet, T., et al. (2018). Single-cell sequencing reveals the origin and the order of mutation acquisition in T-cell acute lymphoblastic leukemia. Leukemia. Published online April 18, 2018. https://doi.org/10.1038/s41375-018-0127-8.

De Keersmaecker, K., Real, P.J., Gatta, G.D., Palomero, T., Sulis, M.L., Tosello, V., Van Vlierberghe, P., Barnes, K., Castillo, M., Sole, X., et al. (2010). The TLX1 oncogene drives aneuploidy in T cell transformation. Nat. Med. *16*, 1321–1327.

De Kouchkovsky, I., and Abdul-Hay, M. (2016). 'Acute myeloid leukemia: A comprehensive review and 2016 update'. Blood Cancer J. *6*, e441.

Del Bianco, C., Vedenko, A., Choi, S.H., Berger, M.F., Shokri, L., Bulyk, M.L., and Blacklow, S.C. (2010). Notch and MAML-1 complexation do not detectably alter the DNA binding specificity of the transcription factor CSL. PLoS ONE *5*, e15034.

Draheim, K.M., Hermance, N., Yang, Y., Arous, E., Calvo, J., and Kelliher, M.A. (2011). A DNA-binding mutant of TAL1 cooperates with LMO2 to cause T cell leukemia in mice. Oncogene *30*, 1252–1260.

DuBridge, R.B., Tang, P., Hsia, H.C., Leong, P.M., Miller, J.H., and Calos, M.P. (1987). Analysis of mutation in human cells by using an Epstein-Barr virus shuttle system. Mol. Cell. Biol. *7*, 379–387.

Fabregat, A., Jupe, S., Matthews, L., Sidiropoulos, K., Gillespie, M., Garapati, P., Haw, R., Jassal, B., Korninger, F., May, B., et al. (2018). The Reactome Pathway Knowledgebase. Nucleic Acids Res. *46* (D1), D649–D655.

Felix, C.A., and Lange, B.J. (1999). Leukemia in infants. Oncologist *4*, 225–240.

Gautier, L., Cope, L., Bolstad, B.M., and Irizarry, R.A. (2004). affy–analysis of Affymetrix GeneChip data at the probe level. Bioinformatics *20*, 307–315.

Geiger, H., de Haan, G., and Florian, M.C. (2013). The ageing haematopoietic stem cell compartment. Nat. Rev. Immunol. *13*, 376–389.

George, J., Uyar, A., Young, K., Kuffler, L., Waldron-Francis, K., Marquez, E., Ucar, D., and Trowbridge, J.J. (2016). Leukaemia cell of origin identified by chromatin landscape of bulk tumour cells. Nat. Commun. *7*, 12166.

Giambra, V., Jenkins, C.R., Wang, H., Lam, S.H., Shevchuk, O.O., Nemirovsky, O., Wai, C., Gusscott, S., Chiang, M.Y., Aster, J.C., et al. (2012). NOTCH1 promotes T cell leukemia-initiating activity by RUNX-mediated regulation of PKC-θ and reactive oxygen species. Nat. Med. *18*, 1693–1698.

Giambra, V., Jenkins, C.E., Lam, S.H., Hoofd, C., Belmonte, M., Wang, X., Gusscott, S., Gracias, D., and Weng, A.P. (2015). Leukemia stem cells in T-ALL require active Hif1α and Wnt signaling. Blood *125*, 3917–3927.

Gusscott, S., Jenkins, C.E., Lam, S.H., Giambra, V., Pollak, M., and Weng, A.P. (2016). IGF1R derived PI3K/AKT signaling maintains growth in a subset of human T-cell acute lymphoblastic leukemias. PLoS ONE *11*, e0161158.

Gutierrez, A., Pan, L., Groen, R.W.J., Baleydier, F., Kentsis, A., Marineau, J., Grebliunaite, R., Kozakewich, E., Reed, C., Pflumio, F., et al. (2014). Phenothiazines induce PP2A-mediated apoptosis in T cell acute lymphoblastic leukemia. J. Clin. Invest. *124*, 644–655.

Herranz, D., Ambesi-Impiombato, A., Sudderth, J., Sánchez-Martín, M., Belver, L., Tosello, V., Xu, L., Wendorff, A.A., Castillo, M., Haydu, J.E., et al. (2015). Metabolic reprogramming induces resistance to anti-NOTCH1 therapies in T cell acute lymphoblastic leukemia. Nat. Med. *21*, 1182–1189.

Holzenberger, M., Leneuve, P., Hamard, G., Ducos, B., Perin, L., Binoux, M., and Le Bouc, Y. (2000). A targeted partial invalidation of the insulin-like growth factor I receptor gene in mice causes a postnatal growth deficit. Endocrinology *141*, 2557–2566.

Homminga, I., Pieters, R., Langerak, A.W., de Rooi, J.J., Stubbs, A., Verstegen, M., Vuerhard, M., Buijs-Gladdines, J., Kooi, C., Klous, P., et al. (2011). Integrated transcript and genome analyses reveal NKX2-1 and MEF2C as potential oncogenes in T cell acute lymphoblastic leukemia. Cancer Cell *19*, 484–497.

Horton, S.J., Jaques, J., Woolthuis, C., van Dijk, J., Mesuraca, M., Huls, G., Morrone, G., Vellenga, E., and Schuringa, J.J. (2013). MLL-AF9-mediated immortalization of human hematopoietic cells along different lineages changes during ontogeny. Leukemia *27*, 1116–1126.

Hu, Y., and Smyth, G.K. (2009). ELDA: Extreme limiting dilution analysis for comparing depleted and enriched populations in stem cell and other assays. J. Immunol. Methods *347*, 70–78.

Kanzler, H., Küppers, R., Hansmann, M.L., and Rajewsky, K. (1996). Hodgkin and Reed-Sternberg cells in Hodgkin's disease represent the outgrowth of a dominant tumor clone derived from (crippled) germinal center B cells. J. Exp. Med. *184*, 1495–1505.

Kim, I., Saunders, T.L., and Morrison, S.J. (2007). Sox17 dependence distinguishes the transcriptional regulation of fetal from adult hematopoietic stem cells. Cell *130*, 470–483.

Konze, K.D., Ma, A., Li, F., Barsyte-Lovejoy, D., Parton, T., Macnevin, C.J., Liu, F., Gao, C., Huang, X.-P., Kuznetsova, E., et al. (2013). An orally bioavailable chemical probe of the Lysine Methyltransferases EZH2 and EZH1. ACS Chem. Biol. *8*, 1324–1334.

Krivtsov, A.V., Figueroa, M.E., Sinha, A.U., Stubbs, M.C., Feng, Z., Valk, P.J.M., Delwel, R., Döhner, K., Bullinger, L., Kung, A.L., et al. (2013). Cell of origin determines clinically relevant subtypes of MLL-rearranged AML. Leukemia *27*, 852–860.

LeRoith, D., and Roberts, C.T., Jr. (1991). Insulin-like growth factor I (IGF-I): A molecular basis for endocrine versus local action? Mol. Cell. Endocrinol. *77*, C57–C61.

Li, H., and Durbin, R. (2009). Fast and accurate short read alignment with Burrows-Wheeler transform. Bioinformatics *25*, 1754–1760.

Lorzadeh, A., Bilenky, M., Hammond, C., Knapp, D.J.H.F., Li, L., Miller, P.H., Carles, A., Heravi-Moussavi, A., Gakkhar, S., Moksa, M., et al. (2016). Nucleosome density ChIP-seq identifies distinct chromatin modification signatures associated with MNase accessibility. Cell Rep. *17*, 2112–2124.

Löwenberg, B., van Putten, W., Theobald, M., Gmür, J., Verdonck, L., Sonneveld, P., Fey, M., Schouten, H., de Greef, G., Ferrant, A., et al.; Dutch-Belgian Hemato-Oncology Cooperative Group; Swiss Group for Clinical Cancer Research (2003). Effect of priming with granulocyte colony-stimulating factor on the outcome of chemotherapy for acute myeloid leukemia. N. Engl. J. Med. *349*, 743–752.

Lund, K., Adams, P.D., and Copland, M. (2014). EZH2 in normal and malignant hematopoiesis. Leukemia *28*, 44–49.

Man, N., Sun, X.-J., Tan, Y., García-Cao, M., Liu, F., Cheng, G., Hatlen, M., Xu, H., Shah, R., Chastain, N., et al. (2016). Differential role of Id1 in MLL-AF9-driven leukemia based on cell of origin. Blood *127*, 2322–2326.

Medyouf, H., Gao, X., Armstrong, F., Gusscott, S., Liu, Q., Gedman, A.L., Matherly, L.H., Schultz, K.R., Pflumio, F., You, M.J., and Weng, A.P. (2010).

Acute T-cell leukemias remain dependent on Notch signaling despite PTEN and INK4A/ARF loss. Blood *115*, 1175–1184.

Medyouf, H., Gusscott, S., Wang, H., Tseng, J.-C., Wai, C., Nemirovsky, O., Trumpp, A., Pflumio, F., Carboni, J., Gottardis, M., et al. (2011). High-level IGF1R expression is required for leukemia-initiating cell activity in T-ALL and is supported by Notch signaling. J. Exp. Med. *208*, 1809–1822.

Meinken, J., Walker, G., Cooper, C.R., and Min, X.J. (2015). MetazSecKB: The human and animal secretome and subcellular proteome knowledgebase. Database (Oxford). Published online August 8, 2015. https://doi.org/10.1093/database/bav077.

Minowada, J., Onuma, T., and Moore, G.E. (1972). Rosette-forming human lymphoid cell lines. I. Establishment and evidence for origin of thymus-derived lymphocytes. J. Natl. Cancer Inst. *49*, 891–895.

Mold, J.E., Venkatasubrahmanyam, S., Burt, T.D., Michaëlsson, J., Rivera, J.M., Galkina, S.A., Weinberg, K., Stoddart, C.A., and McCune, J.M. (2010). Fetal and adult hematopoietic stem cells give rise to distinct T cell lineages in humans. Science *330*, 1695–1699.

Morikawa, S., Tatsumi, E., Baba, M., Harada, T., and Yasuhira, K. (1978). Two E-rosette-forming lymphoid cell lines. Int. J. Cancer *21*, 166–170.

Morita, S., Kojima, T., and Kitamura, T. (2000). Plat-E: An efficient and stable system for transient packaging of retroviruses. Gene Ther. *7*, 1063–1066.

Notta, F., Zandi, S., Takayama, N., Dobson, S., Gan, O.I., Wilson, G., Kaufmann, K.B., McLeod, J., Laurenti, E., Dunant, C.F., et al. (2016). Distinct routes of lineage development reshape the human blood hierarchy across ontogeny. Science *351*. Published online January 8, 2016. https://doi.org/10.1126/science.aab2116.

Ntziachristos, P., Tsirigos, A., Welstead, G.G., Trimarchi, T., Bakogianni, S., Xu, L., Loizou, E., Holmfeldt, L., Strikoudis, A., King, B., et al. (2014). Contrasting roles of histone 3 lysine 27 demethylases in acute lymphoblastic leukaemia. Nature *514*, 513–517.

Oshima, M., Hasegawa, N., Mochizuki-Kashio, M., Muto, T., Miyagi, S., Koide, S., Yabata, S., Wendt, G.R., Saraya, A., Wang, C., et al. (2016). Ezh2 regulates the Lin28/let-7 pathway to restrict activation of fetal gene signature in adult hematopoietic stem cells. Exp. Hematol. *44*, 282–296.

Pabst, T., Vellenga, E., van Putten, W., Schouten, H.C., Graux, C., Vekemans, M.-C., Biemond, B., Sonneveld, P., Passweg, J., Verdonck, L., et al.; Dutch-Belgian Hemato-Oncology Cooperative Group (HOVON); German AML Study Group (AMLSG); Swiss Collaborative Group for Clinical Cancer Research (SAKK) (2012). Favorable effect of priming with granulocyte colony-stimulating factor in remission induction of acute myeloid leukemia restricted to dose escalation of cytarabine. Blood *119*, 5367–5373.

Palomero, T., Barnes, K.C., Real, P.J., Glade Bender, J.L., Sulis, M.L., Murty, V.V., Colovai, A.I., Balbin, M., and Ferrando, A.A. (2006). CUTLL1, a novel human T-cell lymphoma cell line with t(7;9) rearrangement, aberrant NOTCH1 activation and high sensitivity to gamma-secretase inhibitors. Leukemia *20*, 1279–1287.

Park, C.Y. (2016). Context matters in MLL-AF9-driven leukemias. Blood *127*, 2268–2269.

Park, F., Ohashi, K., Chiu, W., Naldini, L., and Kay, M.A. (2000). Efficient lentiviral transduction of liver requires cell cycling in vivo. Nat. Genet. *24*, 49–52.

Pear, W.S., and Radtke, F. (2003). Notch signaling in lymphopoiesis. Semin. Immunol. *15*, 69–79.

Pear, W.S., Aster, J.C., Scott, M.L., Hasserjian, R.P., Soffer, B., Sklar, J., and Baltimore, D. (1996). Exclusive development of T cell neoplasms in mice transplanted with bone marrow expressing activated Notch alleles. J. Exp. Med. *183*, 2283–2291.

Perou, C.M., Sørlie, T., Eisen, M.B., van de Rijn, M., Jeffrey, S.S., Rees, C.A., Pollack, J.R., Ross, D.T., Johnsen, H., Akslen, L.A., et al. (2000). Molecular portraits of human breast tumours. Nature *406*, 747–752.

Petruk, S., Cai, J., Sussman, R., Sun, G., Kovermann, S.K., Mariani, S.A., Calabretta, B., McMahon, S.B., Brock, H.W., Iacovitti, L., and Mazo, A. (2017). Delayed accumulation of H3K27me3 on nascent DNA is essential for recruitment of transcription factors at early stages of stem cell differentiation. Mol. Cell *66*, 247–257.e5.

Pietras, E.M., Warr, M.R., and Passegué, E. (2011). Cell cycle regulation in hematopoietic stem cells. J. Cell Biol. *195*, 709–720.

Piovan, E., Yu, J., Tosello, V., Herranz, D., Ambesi-Impiombato, A., Da Silva, A.C., Sanchez-Martin, M., Perez-Garcia, A., Rigo, I., Castillo, M., et al. (2013). Direct reversal of glucocorticoid resistance by AKT inhibition in acute lymphoblastic leukemia. Cancer Cell *24*, 766–776.

Ritchie, M.E., Phipson, B., Wu, D., Hu, Y., Law, C.W., Shi, W., and Smyth, G.K. (2015). limma powers differential expression analyses for RNA-sequencing and microarray studies. Nucleic Acids Res. *43*, e47–e47.

Saito, Y., Uchida, N., Tanaka, S., Suzuki, N., Tomizawa-Murasawa, M., Sone, A., Najima, Y., Takagi, S., Aoki, Y., Wake, A., et al. (2010). Induction of cell cycle entry eliminates human leukemia stem cells in a mouse model of AML. Nat. Biotechnol. *28*, 275–280.

Schmitt, T.M., and Zúñiga-Pflücker, J.C. (2002). Induction of T cell development from hematopoietic progenitor cells by delta-like-1 in vitro. Immunity *17*, 749–756.

Snoeck, H.-W. (2013). Aging of the hematopoietic system. Curr. Opin. Hematol. *20*, 355–361.

Sutton, R.E., Reitsma, M.J., Uchida, N., and Brown, P.O. (1999). Transduction of human progenitor hematopoietic stem cells by human immunodeficiency virus type 1-based vectors is cell cycle dependent. J. Virol. *73*, 3649–3660.

Szymczak, A.L., Workman, C.J., Wang, Y., Vignali, K.M., Dilioglou, S., Vanin, E.F., and Vignali, D.A.A. (2004). Correction of multi-gene deficiency in vivo using a single 'self-cleaving' 2A peptide-based retroviral vector. Nat. Biotechnol. *22*, 589–594.

Terwilliger, T., and Abdul-Hay, M. (2017). Acute lymphoblastic leukemia: A comprehensive review and 2017 update. Blood Cancer J. *7*, e577.

Tremblay, M., Tremblay, C.S., Herblot, S., Aplan, P.D., Hébert, J., Perreault, C., and Hoang, T. (2010). Modeling T-cell acute lymphoblastic leukemia induced by the SCL and LMO1 oncogenes. Genes Dev. *24*, 1093–1105.

Visvader, J.E. (2011). Cells of origin in cancer. Nature *469*, 314–322.

Wang, H., Zang, C., Taing, L., Arnett, K.L., Wong, Y.J., Pear, W.S., Blacklow, S.C., Liu, X.S., and Aster, J.C. (2014). NOTCH1-RBPJ complexes drive target gene expression through dynamic interactions with superenhancers. Proc. Natl. Acad. Sci. USA *111*, 705–710.

Wang, J., Wissink, E.M., Watson, N.B., Smith, N.L., Grimson, A., and Rudd, B.D. (2016). Fetal and adult progenitors give rise to unique populations of CD8+ T cells. Blood *128*, 3073–3082.

Wendorff, A.A., Koch, U., Wunderlich, F.T., Wirth, S., Dubey, C., Brüning, J.C., MacDonald, H.R., and Radtke, F. (2010). Hes1 is a critical but context-dependent mediator of canonical Notch signaling in lymphocyte development and transformation. Immunity *33*, 671–684.

Weng, A.P., Ferrando, A.A., Lee, W., Morris, J.P., 4th, Silverman, L.B., Sanchez-Irizarry, C., Blacklow, S.C., Look, A.T., and Aster, J.C. (2004). Activating mutations of NOTCH1 in human T cell acute lymphoblastic leukemia. Science *306*, 269–271.

Yost, A.J., Shevchuk, O.O., Gooch, R., Gusscott, S., You, M.J., Ince, T.A., Aster, J.C., and Weng, A.P. (2013). Defined, serum-free conditions for in vitro culture of primary human T-ALL blasts. Leukemia *27*, 1437–1440.

Yu, V.W.C., Yusuf, R.Z., Oki, T., Wu, J., Saez, B., Wang, X., Cook, C., Baryawno, N., Ziller, M.J., Lee, E., et al. (2016). Epigenetic Memory Underlies Cell-Autonomous Heterogeneous Behavior of Hematopoietic Stem Cells. Cell *167*, 1310–1322.e17.

Yuan, J., Nguyen, C.K., Liu, X., Kanellopoulou, C., and Muljo, S.A. (2012). Lin28b reprograms adult bone marrow hematopoietic progenitors to mediate fetal-like lymphopoiesis. Science *335*, 1195–1200.

Zhang, Y., Liu, T., Meyer, C.A., Eeckhoute, J., Johnson, D.S., Bernstein, B.E., Nusbaum, C., Myers, R.M., Brown, M., Li, W., and Liu, X.S. (2008). Model-based analysis of ChIP-Seq (MACS). Genome Biol. *9*, R137.

STAR★METHODS

KEY RESOURCES TABLE

REAGENT or RESOURCE	SOURCE	IDENTIFIER
Antibodies		
Biotin anti-mouse CD3ε antibody (clone 145-2C11)	BioLegend	Cat# 100304; RRID:AB_312669
Biotin anti-mouse CD8a antibody (clone 53-6.7)	BioLegend	Cat# 100704; RRID:AB_312743
Biotin anti-mouse Ly-6G/Ly-6C (Gr-1) antibody (clone RB6-8C5)	BioLegend	Cat# 108404; RRID:AB_313369
Biotin anti-mouse TER-119 antibody (clone TER-119)	BD Biosciences	Cat# 553672; RRID:AB_394985
Biotin anti-human/mouse CD45R (B220) antibody (clone RA3-6B2)	eBioscience, Thermo Fisher Scientific	Cat# 13-0452-85; RRID:AB_466450
Biotin anti-mouse/human CD11b (Mac-1) antibody (clone M1/70)	BioLegend	Cat# 101204; RRID:AB_312787
Biotin anti-mouse CD11c antibody (clone N418)	eBioscience, Thermo Fisher Scientific	Cat# 13-0114-82; RRID:AB_466363
Biotin anti-mouse NK-1.1 antibody (clone PK136)	BioLegend	Cat# 108704; RRID:AB_313391
Streptavidin PE	eBioscience, Thermo Fisher Scientific	Cat# 12-4317-87
APC anti-human CD271 (NGFR) antibody (clone ME20.4)	BioLegend	Cat# 345108; RRID:AB_10645515
APC anti-human CD34 antibody (clone 581)	BioLegend	Cat# 343510; RRID:AB_1877153
APC/Cy7 anti-mouse/human CD11b (Mac-1) antibody (clone M1/70)	BioLegend	Cat# 101225; RRID:AB_830641
PerCP/Cy5.5 anti-mouse Ly-6G/Ly-6C (Gr-1) antibody (clone RB6-8C5)	BioLegend	Cat # 108427; RRID:AB_893561
Anti-Ezh2 antibody (clone D2C9)	Cell Signaling Technologies	Cat# 5246; RRID:AB_1069468
Anti-NOTCH1 antibody (C-20)	Santa Cruz Biotechnology	Cat# sc-6014-R; RRID:AB_650335
Anti-H3K4me3 antibody (clone C42D8)	Cell Signaling Technologies	Cat# 9751; RRID:AB_2616028
Anti-H3K27me3 (lot A1824D)	Diagenode	Cat# C15410069 (pAb-069-050); RRID:AB_2616049
Normal rabbit IgG	Cell Signaling Technologies	Cat# 2729; RRID:AB_1031062
Anti-mouse β-Actin antibody (clone AC-15)	Sigma Aldrich	Cat# A1978; RRID:AB_476692
Biological Samples		
Patient-derived xenograft (PDX) M18	Lab of Françoise Pflumio; Armstrong et al., 2009 and Medyouf et al., 2010	N/A
PDX F1313	Lab of Andrew Weng; Medyouf et al., 2010	N/A
PDX H3255	Lab of Andrew Weng; Yost et al., 2013	N/A
Human cord blood	BC Children's and Women's Hospital	N/A
Chemicals, Peptides, and Recombinant Proteins		
Polyethylenimine, Linear, MW 25000, Transfection Grade (PEI 25K)	Polysicences, Inc	Cat# 23966-1; CAS: 9002-98-6, 26913-06-4
Hexadimethrine bromide (polybrene)	Sigma-Aldrich	Cat# H9268; CAS: 28728-55-4
Propidium iodide	Sigma-Aldrich	Cat# P4170; CAS: 25535-16-4
DAPI	Calbiochem, EMD Millipore	Cat# 268298; CAS: 28718-90-3
TO-PRO-3	Thermo Fisher Scientific	Cat# T3605
Hoechst 33342	Sigma-Aldrich	Cat# B2261; CAS: 23491-52-3
Pyronin Y	Sigma-Aldrich	Cat# 213519; CAS: 92-32-0
UNC1999	Cayman Chemicals	Cat# 14621; CAS: 1431612-23-5
UNC2400	Tocris	Cat# 4905; CAS: 1433200-49-7
γ-Secretase Inhibitor XXI, Compound E	Calbiochem, EMD Millipore	Cat# 565790; CAS: 209986-17-4
Recombinant human IGF-1	PeproTech	Cat# 100-11

(*Continued on next page*)

Continued

REAGENT or RESOURCE	SOURCE	IDENTIFIER
Recombinant human SCF	PeproTech	Cat# 300-07
Recombinant human FLT3-Ligand	PeproTech	Cat# 300-19
Recombinant human IL-2	PeproTech	Cat# 200-02
Recombinant human IL-7	PeproTech	Cat# 200-07
Recombinant human TPO	PeproTech	Cat# 300-18
Recombinant human IGF2	PeproTech	Cat# 100-12
Recombinant human FGFa	PeproTech	Cat# 100-17A
StemRegenin1 (SR1)	StemCell Technologies	Cat# 72342; CAS: 1227633-49-9
BIT 9500 serum substitute	StemCell Technologies	Cat# 09500
Fibronectin	StemCell Technologies	Car# 07159
Recombinant murine IGF-1	PeproTech	Cat# 250-19
Recombinant murine IL-3	PeproTech	Cat# 213-13
Recombinant murine IL-6	PeproTech	Cat# 216-16
Recombinant murine FLT3-Ligand	PeproTech	Cat# 250-31L
Recombinant murine SCF	PeproTech	Cat# 250-03
Recombinant murine IL-2	PeproTech	Cat# 212-12
Recombinant murine IL-7	PeproTech	Cat# 217-17
Critical Commercial Assays		
Mouse/Rat IGF-I DuoSet ELISA	R&D Systems	Cat# DY791
Deposited Data		
Affymetrix gene expression microarray data	This paper; Mendeley Data	https://doi.org/10.17632/3kkc9yp8k7.1
Raw and processed H3K27me3 ChIP-seq data of mouse bone marrow and fetal liver	This paper	GEO: GSE118308
NOTCH/CSL1/RUNX1 ChIP-seq of CUTLL1 cell line	Wang et al., 2014	GEO: GSE51800
Affymetrix gene expression microarray (HG-U133 Plus 2.0) of T-ALL patient samples	Homminga et al., 2011	GEO: GSE26713
Affymetrix gene expression microarray (HG-U133 Plus 2.0) of T-ALL patient samples	Piovan et al., 2013	GEO: GSE32215
Genome Reference Consortium Human Build 37, GRCh37 (hg19)	Genome Reference Consortium	https://www.ncbi.nlm.nih.gov/assembly/GCF_000001405.13/
Genome Reference Consortium Mouse Build 38, GRCm38 (mm10)	Genome Reference Consortium	https://www.ncbi.nlm.nih.gov/assembly/GCF_000001635.20/
Genome Reference Consortium Mouse Build 37, MGSCv37 (mm9)	Genome Reference Consortium	https://www.ncbi.nlm.nih.gov/assembly/GCF_000001635.18/
Experimental Models: Cell Lines		
Human: HEK293T	Lab of Jon Aster; DuBridge et al., 1987	RRID:CVCL_0063
Human: Plat-E	Lab of Françoise Pflumio; Morita et al., 2000	RRID:CVCL_B488
Mouse: MS5-DL1	Lab of Françoise Pflumio; Armstrong et al., 2009	N/A
Mouse: OP9-DL1	Lab of Juan Carlos Zúñiga-Pflücker; Schmitt and Zúñiga-Pflücker, 2002	RRID:CVCL_B218
Human: CUTLL1	Lab of Adolfo Ferrando; Palomero et al., 2006	RRID:CVCL_4966
Human: HPB-ALL	Lab of Jon Aster; Morikawa et al., 1978	RRID:CVCL_1820
Human: MOLT-4	Lab of Jon Aster; Minowada et al., 1972	RRID:CVCL_0013
Mouse: 144CLP	Lab of Jon Aster; Gutierrez et al., 2014	N/A
Experimental Models: Organisms/Strains		
Mouse: IGF1Rneo/neo	Holzenberger et al., 2000	N/A
Mouse: C57BL/6J	In house colony	RRID:IMSR_JAX:000664
Mouse: NOD.Cg-Prkdcscid Il2rgtm1Wjl/SzJ (NSG)	In house colony	RRID:IMSR_JAX:005557

(*Continued on next page*)

Continued

REAGENT or RESOURCE	SOURCE	IDENTIFIER
Oligonucleotides		
TaqMan Gene Expression Assay: IGF1 (FAM), Mouse	Applied Biosystems, Thermo Fisher Scientific	Cat# 4331182; Mm00439560_m1
TaqMan Gene Expression Assay: IGF1 (FAM), Human	Applied Biosystems, Thermo Fisher Scientific	Cat# 4331182; Hs01547656_m1
TaqMan Gene Expression Assay: B2M (VIC, primer limited), Human	Applied Biosystems, Thermo Fisher Scientific	Cat# 4448484; Hs99999907_m1
TaqMan Gene Expression Assay: EZH2 (FAM), Human	Applied Biosystems, Thermo Fisher Scientific	Cat# 4331182; Hs01016789_m1
TaqMan Gene Expression Assay: EZH2 (FAM), Mouse	Applied Biosystems, Thermo Fisher Scientific	Cat# 4331182; Mm00468464_m1
TaqMan Gene Expression Assay: B2M (VIC, primer limited), Mouse	Applied Biosystems, Thermo Fisher Scientific	Cat# 4448484; Mm00437762_m1
Primers for local ChIP-PCR, see Table S9	This paper	N/A
Recombinant DNA		
pLKO.1-shEZH2-43-NGFR	This paper	Derived from Addgene Plasmid #8453 and Broad RNAi Consortium shEZH2 TRCN0000039043
pLKO.1-shEzh2-06-NGFR	This paper	Derived from Addgene Plasmid #8453 and Broad RNAi Consortium shEzh2 TRCN0000304506
pLKO.1-shEzh2-34-NGFR/pLKO.1-shEZH2-34-NGFR	This paper	Derived from Addgene Plasmid #8453 and Broad RNAi Consortium shEzH2/EZH2 TRCN0000301834
pLKO.1-shScr-NGFR	This paper	Derived from Addgene Plasmid #1864
MIG-R1 NOTCH1dE	Lab of Jon Aster	N/A
pRRL-MNDU3-PGK-GFP	Giambra et al., 2012	N/A
pRRL-MNDU3-PGK-NGFR	Gusscott et al., 2016	N/A
pRRL-MNDU3-NOTCH1dE-PGK-GFP	This paper	N/A
pRRL-MNDU3-IGF1R(CA)-PGK-NGFR	Gusscott et al., 2016	N/A
pRRL-MNDU3-IGF1R(CAKD)-PGK-NGFR	Gusscott et al., 2016	N/A
pRRL-MNDU3-NOTCH1dE-2A-GFP	This paper	N/A
pRRL-MNDU3-LMO2-2A-TAL1-2A-Cherry	This paper	N/A
pRRL-MNDU3-LMO2-2A-TAL1-2A-BMI1-2A-Cherry	This paper	N/A
Software and Algorithms		
FlowJo v10	FlowJo, LLC	RRID:SCR_008520
GraphPad Prism v7	GraphPad Software	RRID:SCR_002798
QuantaSoft Software v1.7.4	Bio-Rad Laboratories	N/A
Image Studio Lite v4.0.21	LI-COR Biosciences	RRID:SCR_014211
Reactome	Fabregat et al., 2018	RRID:SCR_003485
BWA-backtrack v0.5.7	Li and Durbin, 2009	RRID:SCR_010910 (https://github.com/lh3/bwa)
BAM2WIG	N/A	RRID:SCR_015697 (https://github.com/MikeAxtell/bam2wig)
MACS2 v2.1.0	Zhang et al., 2008	RRID:SCR_013291 (https://github.com/taoliu/MACS)
ELDA: Extreme Limiting Dilution Analysis	Hu and Smyth, 2009	http://bioinf.wehi.edu.au/software/elda/
Bioconductor limma package	Ritchie et al., 2015	RRID:SCR_010943; https://doi.org/10.18129/B9.bioc.limma
Bioconductor affy package	Gautier et al., 2004	https://doi.org/10.18129/B9.bioc.affy

(*Continued on next page*)

Continued

REAGENT or RESOURCE	SOURCE	IDENTIFIER
Other		
EasySep human CD34 positive selection kit	STEMCELL Technologies	Cat# 18056
StemPro-34 media	GIBCO, Thermo Fisher Scientific	Cat# 10639011
StemSpan SFEM II	STEMCELL Technologies	Cat# 09605
StemSpan Lymphoid Progenitor Expansion Supplement	STEMCELL Technologies	Cat# 09915
StemSpan Lymphoid Differentiation Coating Material	STEMCELL Technologies	Cat# 09925

CONTACT FOR REAGENT AND RESOURCE SHARING

Further information and requests for resources and reagents should be directed to and will be fulfilled by the Lead Contact, Andrew Weng (aweng@bccrc.ca). MS5-DL1, OP9-DL1, and CUTLL1 cells were obtained under MTAs with INSERM, University of Toronto, and Columbia University, respectively.

EXPERIMENTAL MODEL AND SUBJECT DETAILS

Mice

Animals were housed in a specific pathogen-free facility and experiments were performed under approved BCCA/UBC institutional review board protocols according to Canadian Council on Animal Care (CCAC) guidelines. Syngeneic (C57BL/6; RRID:IMSR_JAX:000664) transplant recipient mice were 8-13 weeks of age. Immunodeficient (NOD.Cg-*Prkdc*^{scid} *Il2rg*^{tm1Wjl}/SzJ, or NSG; RRID:IMSR_JAX:005557) xenograft recipient mice were 7-17 weeks of age. Male and female animals were represented in balanced proportion when in-house colony stock availability necessitated using mixed sex recipients.

Primary mouse HSPC cultures

All mouse donor tissues were obtained from either wild-type C57BL/6 mice or IGF1R$^{neo/neo}$ mice (Holzenberger et al., 2000) that have been backcrossed over 20 generations to C57BL/6. Fetal liver (FL) tissues were obtained from embryonic day (e) 14.5 fetuses. The sex of e14.5 fetal liver donors is unknown as anatomic differences are not apparent at this early stage of development; however, livers from 8-12 e14.5 fetuses across 2-3 gravid females were pooled for each experiment. Bone marrow (BM) tissues were harvested from 8 week old adult mice. BM from 6-8 mice with male and female donors in equal proportion were pooled for each experiment. These same mouse FL and BM tissues were used as donor material in transplantation studies to generate mouse tissue-derived leukemias.

Primary human cord blood cultures

Anonymized normal human cord blood (CB) samples were obtained with informed consent from women undergoing caesarian deliveries of full-term births according to protocols approved by the Research Ethics Board of the University of British Columbia and Children's & Women's Hospital of BC. The sex of the CB donors is unknown as these are anonymized samples; however, CB cells from a pool of 255 donors were used for these experiments.

Patient-derived xenografts

Primary human T-ALL samples were obtained with appropriate institutional review board approvals and informed consent under guidelines established by the Declaration of Helsinki. Patient-derived xenografts were established by injection of primary patient biopsy material into sublethally irradiated (200 rad) adult NSG mice as described (Medyouf et al., 2010). The M18, F1313, and H3255 PDX lines have all been reported previously (Medyouf et al., 2010; Yost et al., 2013).

Cell lines

Human cell lines CUTLL1 (Palomero et al., 2006), HPBALL (Morikawa et al., 1978), and MOLT4 (Minowada et al., 1972) were all derived from male T-ALL patients. The sex of HEK293T/Plat-E, MS5-DL1, OP9-DL1, and 144CLP cell lines is unknown as this aspect of their provenance is unclear in the literature. Cell line identities were verified by STR profiling (PowerPlex16; Promega).

METHOD DETAILS

Plasmids

We expressed cDNAs from either retroviral MigR1 (Medyouf et al., 2010) or lentiviral pRRL-cPPT/CTS-MNDU3-PGK-GFP-WPRE vectors (Giambra et al., 2012). Human NOTCH1 (ΔE allele), TAL1, BMI1, and mouse LMO2 cDNAs obtained from Dr. J Aster (Boston), Harvard PlasmID, and Dr. E Lawlor (UCLA). A constitutively active (CA) form of IGF1R (CD8-IGF1R fusion) and its kinase dead (CAKD) mutant (K1003A) were constructed as described (Gusscott et al., 2016). Individual cDNAs within multicistronic constructs were connected with equine rhinitis A virus 2A (E2A), Thosea asigna virus 2A (T2A), and foot-and-mouse disease virus 2A (F2A) peptides

(Szymczak et al., 2004). We expressed shRNAs from the RNAi Consortium against mouse Ezh2/human EZH2 using an NGFR-tagged derivative of the pLKO.1 puro lentivector (Addgene #8453). The scrambled shRNA control vector was also obtained from Addgene (#1864). All constructs were verified by sequencing. Additional vector construction details are available upon request.

Viral transduction

We generated high-titer, replication-defective retrovirus by transient transduction of Plat-E cells with PEI (Medyouf et al., 2011). We generated lentivirus by transient co-transduction of 293T cells with PEI using 2nd generation packaging and envelop vectors, followed by ultracentrifugal concentration (25,000 rpm for 95min @ 4C; Beckman SW 32 Ti rotor) (Giambra et al., 2015). Mouse progenitor cells were transduced by spinoculation (1800 x*g* for 2h @ 33C) with viral supernatants in 4 ug/ml polybrene (Medyouf et al., 2011). Human CB cells were transduced in 96-well plates coated with 5 μg/cm^2 fibronectin (StemCell Technologies) by direct addition of concentrated viral supernatants and incubated at 37C/5% CO2 for 6 hours.

Mouse fetal liver/BM transplantation

To generate primary mouse leukemias, we transduced lineage-negative (lin−) progenitor cells from embryonic day 14.5 fetal liver (FL) or bone marrow (BM) from 8 week old C57BL/6 mice. Briefly, cells were harvested from freshly explanted FL or BM tissues in PBS with 3% FBS, then stained with a lineage panel comprising antibodies against CD3, CD8, Gr1, Ter119, B220, CD11b, CD11c, and NK1.1 (eBioscience, Biolegend). Lin− cells were isolated by fluorescence activated cell sorting (FACS), and then prestimulated overnight in StemPro-34 media (GIBCO) supplemented with 10% FCS, antibiotics, and cytokines IL-3, IL-6, and FLT3 ligand (10 ng/ml each), and SCF (100 ng/ml) (Peprotech). Cells were then transduced by spinoculation with lentivirus at 300x*g* for 2h, and cultured for 3 days in the same media. Transduced GFP+ or NGFR+ cells were then FACS sorted and injected by tail vein into lethally irradiated (810 rad) C57BL/6 recipient mice at doses of 10,000-40,000 transduced cells per mouse, along with a radioprotective dose of least 1×10^5 normal bone marrow cells.

Limit dilution serial transplants were performed by injecting varying doses of established leukemia cells by tail vein into non-irradiated syngeneic C57BL/6 or sublethally irradiated (200 rad) immunodeficient NSG (NOD/Scid/Il2rg$^{-/-}$) recipient mice. Transplanted recipient mice were monitored daily for clinical signs of leukemia development and by periodic sampling of peripheral blood for assessment of engraftment/disease progression by flow cytometry.

Mice developing clinical signs of leukemia were sacrificed and confirmed to show substantial bone marrow and spleen involvement by flow cytometry. Mice that did not develop clinical signs of leukemia were sacrificed at arbitrary assay endpoints (typically beyond 90 days post-transplant) and confirmed to lack leukemia engraftment of bone marrow or spleen by flow cytometry.

Isolation of human progenitor cells

CD34+ CB cells were obtained at > 95% purity from pooled collections using a two-step Rosette-Sep/EasySep human CD34 positive selection kit (StemCell Technologies) according to the manufacturer's protocols and/or FACS sorting (BD FACSAria III, BD FACSFusion). The purity of FACS-sorted cells was > 99% as determined by post-sort analysis. CD34+ cells were seeded into 96-well round bottom plates and pre-stimulated in StemSpan SFEM II (StemCell Technologies) with 10 ng/ml human SCF, 20 ng/ml human TPO, 20 ng/ml human IGF2, and 10 ng/ml human FGFa (Peprotech) for 16 hours.

Cell Culture

We cultured transduced mouse FL or BM cells in StemPro-34 media (GIBCO) supplemented with 10% fetal calf serum (FCS), antibiotics, and cytokines IL-3, IL-6, and FLT3 ligand (10 ng/ml each), and SCF (100 ng/ml) (Peprotech). We cultured freshly explanted mouse leukemia cells in RPMI 1640 media (GIBCO) supplemented with 20% FCS, 1mM sodium pyruvate, 2mM GlutaMAX (GIBCO), antibiotics, and cytokines IL-2 and IL-7 (10 ng/ml each; Peprotech). Human T-ALL cell lines were cultured in RPMI 1640 media supplemented with 10% FCS, with 1mM sodium pyruvate, 2mM GlutaMAX (GIBCO), and antibiotics. Explanted PDX cells were cultured on MS5-DL1 feeders in IMDM (GIBCO) with 10 ng/ml IL-2, 10 ng/ml IL-7 (Peprotech), and 0.75 uM SR1 (StemCell Technologies), except during periods of drug treatment when cells were cultured without feeders in the same media. In some situations, PDX cell culture media was further supplemented with BIT 9500 (StemCell Technologies). CD34+ human cord blood cells were cultured on OP9-DL1 feeders in αMEM with 20% FBS (Invitrogen) plus 10 ng/mL SCF, 5 ng/mL FLT3 ligand and 3 ng/mL IL-7 (Peprotech), or without feeders in StemSpan SFEM II with Lymphoid Progenitor Expansion Supplement and Lymphoid Differentiation Coating Material (StemCell Technologies, cat #09940). The EZH2 inhibitor UNC1999 and its inactive analog UNC2400 were obtained from Cayman Chemical (cat #14621) and Tocris Bioscience (cat #4905), respectively. The γ-secretase inhibitor compound E was obtained from Calbiochem (cat #565790).

Flow Cytometry

We used anti-hCD271 (Miltenyi Biotec, Biolegend) to detect the lentiviral NGFR marker. To assess cycling activity of cells, we stained live cells with 5 μg/ml Hoechst 33342 and 1 μg/ml Pyronin Y (Sigma). Live/dead cell gating was performed by staining with propidum iodide, DAPI, or ToPro3 (Invitrogen). We performed flow cytometric analyses on FACSCalibur/Canto2/LSRFortessa instruments and sorting on FACSVantage DiVa/Aria2/Aria3/Fusion instruments (BD Biosciences). We analyzed flow cytometry data using FlowJo software (TreeStar).

Expression Profiling by Microarray

Total RNA was used for cRNA synthesis and hybridized to Affymetrix Mouse Gene 1.0 ST arrays at the McGill University/Genome Quebec Innovation Centre. For differential gene expression analysis, raw CEL data files were RMA normalized and mapped to ENSEMBL gene IDs using a custom CDF file, version 21 (Dai et al., 2005) with the Bioconductor affy package (Gautier et al., 2004). Differentially expressed genes were then identified using the Bioconductor limma package (Ritchie et al., 2015).

RT-PCR

We lysed cells and extracted total RNA using Trizol reagent (Invitrogen). We generated first strand cDNA by reverse transcription with SuperScript III/VILO master mix (Invitrogen) including a combination of random 15-mer and anchored oligo(dT) primers. We then amplified product by quantitative/real-time PCR (qPCR) using either Taqman probe-based detection with a Dyad Disciple/Chromo4 (Bio-Rad) or StepOnePlus (Applied Biosystems) instrument. We assayed each sample in triplicate and calculated expression levels by the ΔΔCt method with normalization to β-2-microglobulin (B2M) control. Alternatively, we amplified product by Taqman probe-based droplet digital PCR (ddPCR) with a QX200 instrument (Bio-Rad). Absolute quantification analysis was performed using a Poisson algorithm with QuantaSoft software (Bio-Rad) and included normalization to B2M control. We used the following TaqMan probe-based assays: IGF1 (Hs01547656_m1; FAM), *Igf1* (Mm00439560_m1; FAM), EZH2 (Hs01016789_m1; FAM), Ezh2 (Mm00468464_m1; FAM), B2M (Hs99999907_m1; VIC, primer limited) and B2m (Mm00437762_m1; VIC, primer limited) (Applied Biosystems/ThermoFisher).

ELISA

We used a standard ELISA kit to measure mouse IGF1 levels in culture supernatants (cat #DY791, R&D Systems). All assays were performed in triplicate.

Western blot

Whole cell lysates were separated by SDS-PAGE, transferred to Hybond-ECL membranes (Amersham) and blocked with 5% nonfat dry milk. Membranes were probed with primary antibodies against EZH2 (D2C9; Cell Signaling Technology) or β-actin (AC-15; Sigma Aldrich), then with HRP-conjugated secondary antibodies (Jackson ImmunoLaboratories) and detected with enhanced chemiluminescence (ECL; Pierce). Band intensities were quantified with Image Studio Lite (LI-COR) software.

ChIP-PCR

We performed chromatin immunoprecipitation (ChIP) as described previously (Giambra et al., 2012) with the following antibodies: H3K4me3 (cat #9751S, Cell Signaling), H3K27me3 (cat #pAb-069-050, Diagenode), NOTCH1 (cat #sc-6014-R, Santa Cruz Biotechnology), and IgG control (cat #2729, Cell Signaling). DNA was extracted from immunoprecipitated chromatin and assayed by quantitative real time or droplet digital PCR using SYBR- or EvaGreen-based detection, respectively. Primer sequences used for amplification are listed in Table S7.

ChIP-seq

We performed chromatin immunoprecipitation (ChIP) as described previously (Lorzadeh et al., 2016) using a validated anti-H3K27me3 antibody (cat #pAB-195-050, Diagenode). DNA was extracted and NGS libraries were constructed using an Agilent Bravo automated liquid handling platform. Samples were first subjected to End Repair (1x NEB 2 buffer, 1 mM ATP, 0.4 mM dNTP, T4 Polynucleotide Kinase, T4 DNA Polymerase, Klenow DNA Polymerase), then DNA was purified with 23% PEG-Sera Mag Speedbeads (Fisher Scientific) and subjected to A-Tailing (1X NEB 2 buffer, 0.2 mM dATP, Klenow exo minus) at 37C for 30 min. A-Tailed products were purified with 23% PEG-Sera Mag beads. Illumina adaptors were then ligated to A-Tailed products in a 60ul final volume (1X Quick Ligation Buffer, NEB T4 DNA Ligase, 1 uM Illumina sequencing adaptors) at room temperature overnight. Size selection was performed and DNA purified using 20% PEG-Sera Mag Speedbeads. Adaptor-ligated libraries were PCR amplified and barcoded with custom indexing primers (1X High Fidelity buffer, 0.16 mM dNTPs, 2.5% DMSO, 0.83 mM Illumina PCR primer 1.0, 0.83 mM custom indexing primer and 1U Phusion HotStartII). The PCR program included an initial denaturation step at 98C for 30 s, followed by 8 cycles at 98C for 15 s, 65C for 30 s, and 72C for 30 s, and ending with a final step at 72C for 5 min. PCR amplified libraries were sized selected to remove primer dimers and purified with 20% PEG-Sera Mag Speedbeads. Libraries were sequenced on an Illumina HiSeq. Raw sequences were inspected for quality, sample swap and reagent contamination using custom in-house scripts. Read sequences were aligned to NCBI Build 37 (mm9) mouse reference genome using BWA-backtrack v0.5.7 (Li and Durbin, 2009) and default parameters. Custom java program (BAM2WIG) was used to generate wig files for downstream analysis and visualization in genome browser. Reads with BWA mapping quality scores < 5 were discarded and reads that aligned to the same genomic coordinate were counted only once in the profile generation. Peak enrichment was computed using MACS2 v2.1.0 (Zhang et al., 2008) with a false discovery rate (FDR) value of 0.05 and ''–broad'' option for H3K27me3 datasets. To increase the specificity of peak calling, input DNA control samples were analyzed in parallel.

QUANTIFICATION AND STATISTICAL ANALYSIS

All statistical analyses were performed using GraphPad Prism software. The details of these analyses can be found in the respective figure legends. In general, statistical significance was defined by t test or One-way ANOVA for quantitative gene or protein expression

data, or log-rank test for survival data, with cut-offs set at the $p < 0.05$ level. For gene/protein expression data, n indicates the number of replicates, and for survival data, n indicates the number of injected animals. For quantitative ddPCR assessment of gene expression level (RT-ddPCR assays), 95% confidence intervals were plotted as calculated by QuantaSoft version 1.7.4 software (Bio-Rad) using Poisson statistics. LIC frequencies were calculated from limiting dilution transplant results as reported (Hu and Smyth, 2009) using the online ELDA tool available at http://bioinf.wehi.edu.au/software/elda/.

DATA AND SOFTWARE AVAILABILITY

The accession number for the ChIP-seq data reported in this paper (Figure 3E) is GEO: GSE118308.

The Affymetrix gene expression microarray data (Figure 2C) have been deposited in Mendeley Data at https://doi.org/10.17632/3kkc9yp8k7.1.